colloidal allostery

anne weijkamp

Master thesis

Colloidal Allostery

Anne Weijkamp BSc

Under the supervision of:
Jasper Landman MSc
Dr. Burak Eral
Prof. Dr. Willem K. Kegel

Van 't Hoff Laboratory
for Physical and Colloid Chemistry
Utrecht University
Netherlands
January 10, 2017

ABSTRACT

Allostery is a type of adhesion process, where the substrate can be in multiple states, each with a different binding affinity for the adsorbent. Allosteric processes are a fundamental requirement for cell life and better understanding of allostery could therefore lead to a better understanding of biology. The aim of this thesis is to provide with the first steps towards building a model for allosteric interactions on a colloidal scale. We use rigid dyed polystyrene particles binding to elastic poly(ethylene glycol)diacrylate (PEGDA) posts by depletion interaction. A theoretical model is developed, which can provide with insights into realizing colloidal allostery. First steps are then taken to verify this model and proposals are made to further this research.

CONTENTS

1. INTRODUCTION

Adhesion is a very important process in biology. Think for example of the gecko sticking to glass walls, pollen adsorbing to a honey bee or cement dust in the lungs of construction workers [1, 2, 3]. Allostery is a specific type of adhesion process, where the substrate has multiple states and each state has a different affinity for a specific adsorbent. Allostery is a fundamental requirement for cell life, appearing for example in ligand-receptor binding, ligand-gated ion channels, chemotaxis and gene regulation [4, 5, 6].

The history of allostery starts with hemoglobin, of which an illustration can be seen in figure 1.1. Hemoglobin is a protein, present in red blood cells, which contains four subproteins, each containing a binding site with a heme group to which an oxygen molecule can bind reversibly, allowing oxygen to be transported throughout the body [7]. In 1904, Christian Bohr discovered that the concentration of carbon dioxide in the blood affects the binding affinity of oxygen to hemoglobin [8]. In 1961, the term allostery was first coined by Jaques Monod and Francois Jacob [9]. Later in the 1960's, Monod, Wyman, and Changeux developed the MWC model to describe allosteric interactions [10]. It was also Monod who went on to call allostery the "second secret to life", second only to the genetic code [11].

The main application in studying allosteric interactions is understanding the mechanism of biological systems. In the last three years, 1300 scientific papers where published on allostery, showing that allostery has become an emerging but still underappreciated field [6]. By studying allosteric interactions, we could get a little closer to understanding the complex wonder that is biology. Furthermore, studying these interactions could lead to a better general understanding of adhesion processes. In the long run, this could lead to better, more specific filters, aiding in separation and filtration processes.

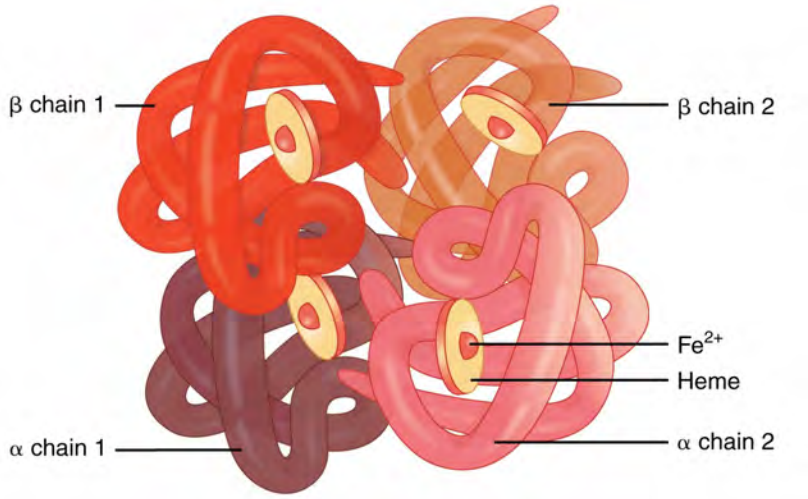

Fig. 1.1: An illustration of hemoglobin, showing the quarternary structure, the four binding sites and their heme groups. Image from [7].

Studying allostery experimentally is difficult, due to the cell being an extremely crowded environment. By building a model for allostery on a colloidal scale, meaning one length scale is roughly on the order of 0.1 µm to 1 µm [12], we could possibly study allosteric interactions *in situ*, using an optical microscope.

This thesis aims to provide with the first steps towards building such a model. We use rigid dyed polystyrene particles binding to elastic poly(ethylene glycol)diacrylate (PEGDA) posts by depletion interaction as our analogy to allostery. First, we develop a theoretical model for the interactions between these components, after which experimental details on the first steps towards verifying this model are discussed. Finally, we provide with a conclusion and suggestions on further research.

2. THEORETICAL BACKGROUND

In this chapter, we start by explaining allosteric processes, using the example of oxygen and hemoglobin (2.1). We then define system we will be using to build a model for allosteric interactions on a colloidal scale and expand on the interactions at play this system (2.2).

2.1 Oxygen and hemoglobin, an allosteric process

Hemoglobin is a protein, present in red blood cells, which contains four binding sites. Each binding site contains a heme group to which an oxygen molecule can bind reversibly, allowing oxygen to be transported throughout the body [7]. As this was the first process that was discovered to be allosteric, it has been the prime example of allostery ever since [8]. We will therefore also use oxygen and hemoglobin as our example.

The fraction of binding sites occupied by oxygen molecules, Θ, can be obtained via the grand canonical ensemble:

$$\Theta = \frac{\langle n \rangle}{4} = \frac{1}{4} \frac{\lambda}{\Xi} \frac{\delta \Xi}{\delta \lambda} \tag{2.1}$$

were Θ is the fraction of occupied binding sites, $\langle n \rangle$ is the average number of bound oxygen molecules (which is divided by 4 since hemoglobin has 4 binding sites), λ is the fugacity, which is an effective concentration, and Ξ is the grand canonical partition function.

If we then take hemoglobin to be a single lattice which can exist only in a single state and has 4 binding sites, the grand canonical partition function is given by:

$$\Xi = (1 + \lambda \mathrm{e}^{-\beta \epsilon n})^4 \tag{2.2}$$

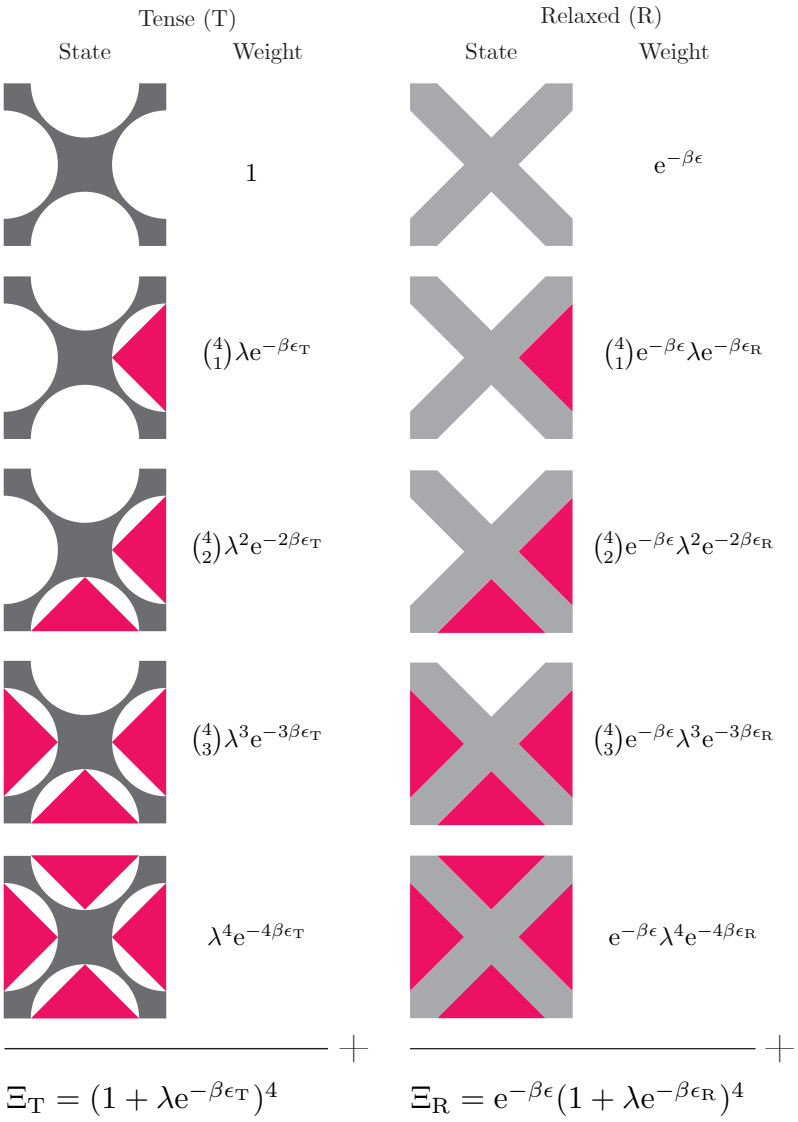

Fig. 2.1: Schematic illustration showing how the grand partition functions Ξ_R and Ξ_T are formed. Adapted from [13].

were ϵ gives the binding energy to the substrate and n gives the number of adsorbed particles. We use β as an abbreviation for the inverse thermal energy $(k_{\mathrm{B}}T)^{-1}$, with k_{B} the Boltzmann constant and T the absolute temperature. Combining equations 2.1 and 2.2 then yields:

$$\Theta = \frac{\lambda \mathrm{e}^{-\beta\epsilon}}{1 + \lambda \mathrm{e}^{-\beta\epsilon}} \tag{2.3}$$

which is the Langmuir adsorption equation for this specific system [13].

However, hemoglobin can exist in two different conformations, commonly referred to as the tense (T) and the relaxed (R) state, illustrated in figure 2.1. The tense state does not cost the hemoglobin energy, but it will be less favourable for the oxygen to bind. Conversely, the relaxed state costs the hemoglobin energy, but it is more favourable for the oxygen to bind [4].

We can derive the equation for the fraction of occupied binding sites in the same way as before, using the grand canonical ensemble, but we have to make a change in the grand canonical partition function Ξ, which is now given by:

$$\begin{aligned} \Xi &= \Xi_{\mathrm{T}} + \Xi_{\mathrm{R}} \\ &= (1 + \lambda \mathrm{e}^{-\beta\epsilon_{\mathrm{T}} n})^4 + \mathrm{e}^{-\beta\epsilon}(1 + \lambda \mathrm{e}^{-\beta\epsilon_{\mathrm{R}} n})^4 \end{aligned} \tag{2.4}$$

This equation looks quite similar to equation 2.2, but with an important difference: ϵ is now the energy needed for the conformation change and ϵ_{T} and ϵ_{R} give the binding energies of the adsorbent to the tense and the relaxed state, respectively. An illustration on how the partition function is built up is shown in figure 2.1.

We can now combine equations 2.1 and 2.1 in the same way as before, yielding

$$\Theta = \Xi^{-1}\{\lambda \mathrm{e}^{-\beta\epsilon_{\mathrm{T}}}(1 + \lambda \mathrm{e}^{-\beta\epsilon_{\mathrm{T}}})^3 + \mathrm{e}^{-\beta\epsilon}\lambda \mathrm{e}^{-\beta\epsilon_{\mathrm{R}}}(1 + \lambda \mathrm{e}^{-\beta\epsilon_{\mathrm{R}}})^3\} \tag{2.5}$$

which is the Monon-Wyman-Changeux (MWC) model for this specific system [4, 14].

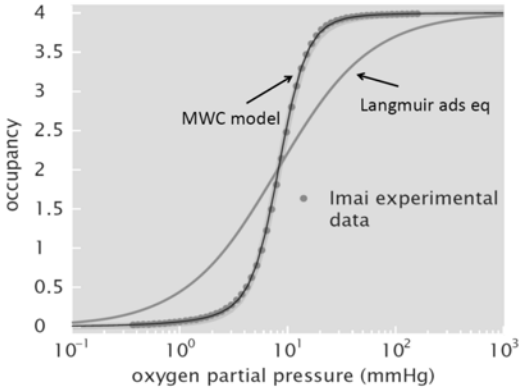

Fig. 2.2: Plot of experimental data, MWC model and Langmuir model, figure obtained from [13], experimental data by Kiyohiro Imai.

When looking at plots of these equations, together with experimental data as required by Kiyoghiro Imai, in figure 2.2, it is obvious that the MWC model fits the experimental data much better.

The MWC model shows a much steeper curve than the Langmuir equation, showing a collective effect of the particles adsorbing onto the substrate. The ability to be in two different conformations leads to a collective "all or nothing" effect. It is favourable to either bind no oxygen at all, resulting in the tense, low energy state of the hemoglobin, or for all binding sites to be occupied. The sum of the energy gained by the binding of the oxygen is then enough to overcome the energy barrier of the hemoglobin being in the tense state [14].

Having this collective effect makes sense from an evolutionary standpoint. Imagine having to transport a lot of bowling balls from Utrecht to Groningen, using transport trucks. You will want to load up every truck to full capacity, in order to transport the bowling balls as efficiently as possible. The collective effect takes care of this in the body: due to the steep curve, there will be very few, if any, hemoglobin molecules that will not have four oxygen molecules bound at normal atmospheric pressures. The collective effect caused by the allosteric interaction thus ensures the most efficient way of transporting oxygen throughout the body.

2.2 A colloidal model

In any allosteric process, there are two competing energies: the energy to bind the adsorbent to the substrate, and the energy to change the conformation of the substrate. We therefore need an adsorbent and a substrate which have this same energy competition for the colloidal model.

We chose rigid polystyrene particles with a diameter of 2 µm as the adsorbent for our system. These particles are large enough to be easily seen with an optical microscope, but small enough to exhibit Brownian motion – that is, their sedimentation can be neglected with respect to their thermal motion [12]. Therefore, they are able to diffuse freely throughout the medium. For this medium, we use a $1\,\mathrm{mmol\,L^{-1}}$ aqueous sodium chloride (NaCl) solution, as the salt will help screen any charge interactions.

As a sample cell, PDMS microfluidic channels were chosen. PDMS microchannels are quick, easy and cheap to manufacture and are widely used for various purposes, such as quick diagnosis of medical issues, studying the behaviour of particles in confined flow and the synthesis of colloidal particles using stop-flow lithography [15, 16, 17]. Most importantly, fluid can flow through them freely. This allows for the *in situ* fabrication of our substrate: deformable PEGDA posts. In chapter 3, more information is provided on the synthesis process of both the particles and the PEGDA posts.

The energy to bind the particle to the substrate will be the depletion interaction (section 2.2.1) and the energy to change the conformation of the substrate will be the elasticity (deformability) of the PEGDA posts (section 2.2.2). In the rest of this section, we will go into both these interactions, add them together (section 2.2.3) and then use them to calculate a theoretical value for the escape time (section 2.2.4).

2.2.1 Binding energy: the depletion interaction

For the binding of the polystyrene sphere to the PEGDA post, a very common tool from the toolbox of the colloid chemist is used: the depletion interaction.

Depletion interaction is an effective attractive force between colloids, which occurs when they are suspended in a medium with a de-

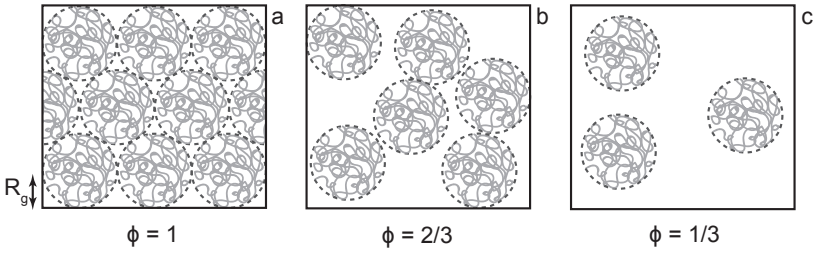

Fig. 2.3: Illustration of the concentration as a fraction of overlap concentration, where in (a) $\phi = 1$, (b) $\phi = 2/3$ and (c) $\phi = 1/3$.

pletant. Depletants typically are very small particles or, as in our case, large polymer molecules. This interaction is illustrated in figure 2.3. Each polymer is fit into an imaginary sphere, with radius R_g. Around the colloids, there is an area where the center of mass of this sphere cannot be: the so-called excluded volume. If these excluded volumes overlap, leading to an overlap volume, this leads to more volume being available to the depletant and as such an increase in entropy. This causes the system to try to maximize the overlap volume, by pushing the colloids together [18].

To be able to use the equations commonly used in colloid chemistry, the concentration needs to be in the diluted regime [12]. This means that the concentration should be below the overlap concentration. At the overlap concentration, the concentration of polymer inside the imaginary sphere with radius R_g is equal to the bulk concentration of polymer in the system. That is, the volume fraction $\phi = 1$. We use this volume fraction ϕ as a measure for concentration throughout this thesis.

Because the particle is so small in comparison to the post (2 µm vs 100 µm), the system can be treated as a rigid particle interacting with a deformable wall. This interaction is illustrated in figure 2.4. The overlap volume in the region where the particle gets close enough to the wall to get an overlap volume, to where the particle is completely encapsulated in the PEGDA wall, is given by:

$$V_O = \frac{1}{3}\pi h_O(d)^2(3(r + R_g) - h_O(d)) \tag{2.6}$$

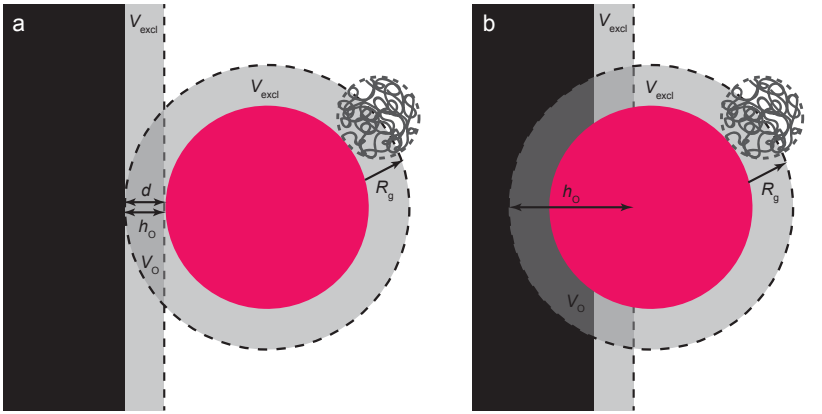

Fig. 2.4: Illustration of a rigid particle interacting with a deformable wall, where in (a) only the excluded volumes of wall and sphere overlap and in (b) the particle deforms the wall.

which is the equation for the volume of a spherical cap of a sphere with radius $r + R_g$, where r is the radius of the particle and R_g is the radius of gyration of the polymer and height $h_O(d)$ as as a function of the distance d between the face of the particle and the wall.

The depletion energy for ideal solutions is then calculated by [12]:

$$W = \Pi V_O = n_b V_O k_B T \tag{2.7}$$

where Π is the osmotic pressure of the depletant V_O the overlap volume as calculated in equation 2.6, n_b the number density of the polymer and $k_B T$ the thermal energy with k_B the Boltzmann constant and T the absolute temperature. The number density n_b is given by

$$n_b = \phi \left(\frac{3}{4} \pi R_g^3 \right)^{-1} \tag{2.8}$$

where ϕ is the volume fraction of polymer and $\left(3/4\pi R_g^3\right)^{-1}$ the volume of the imaginary sphere with radius R_g. This shows that the depletion energy is dependent on the size (R_g) and concentration (ϕ) of the polymer, and the radius (r) of the particle, as a function of the distance to the wall (d).

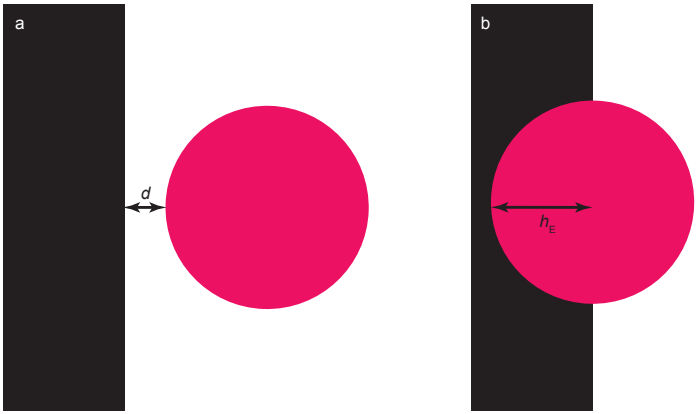

Fig. 2.5: Illustration of a deformable wall and a particle where in (a) the particle approaches and in (b) the particle deforms the wall.

2.2.2 Conformation change: elasticity of the PEGDA posts

It has already been mentioned that the PEGDA posts are deformable. By tuning the elasticity of the post we can tune the energy required for deformation of the post. This deformation forms our model for the conformation change in the substrate.

As mentioned before, the system can be treated as a rigid particle interacting with a deformable wall. This means we can approach it as a Hertzian contact problem of a rigid sphere interacting with an elastic half-space. As the particle deforms the wall more, as illustrated in figure 2.5, the elastic energy will increase. The elastic energy in the region from where the particle touches the wall, to where the particle is completely encapsulated in the PEGDA wall is then given by

$$U = \frac{8}{15} E r^{1/2} h_{\mathrm{E}}(d)^{5/2} \tag{2.9}$$

where E is the elasticity of the post, r is the radius of the particle and $h_{\mathrm{E}}(d)$ is the height of the spherical cap of a sphere with radius r as a function of the distance d between the face of the particle and the wall [19]. This shows that the elastic energy is only dependent on the elasticity (E), as a function of the distance to the wall (d).

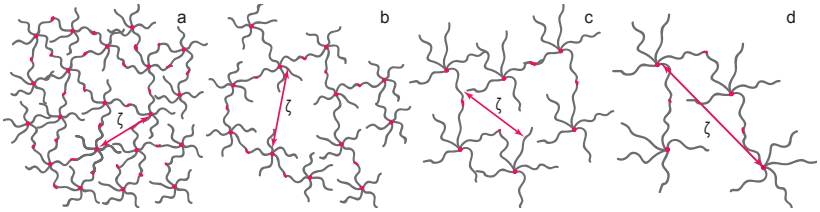

Fig. 2.6: Illustration of PEGDA crosslinking in stars and their characteristic length ζ, with (a) short PEGDA chains and $\phi \approx 1$, (b) short PEGDA chains and $\phi \approx 0,75$, (c) long PEGDA chains and $\phi \approx 1$ and (d) long PEGDA chains and $\phi \approx 0,75$.

The PEGDA posts are hydrogels, which are isotropic Hookean solids. This means that the elasticity, E is given by [20]

$$E = G_0 = G' + iG'' \tag{2.10}$$

where G_0 is the shear elastic modulus, G' is the storage modulus, which represents the elastic portion, and G'' is the loss modulus, which represents the energy being dissipated as heat. This means that by measuring the shear elastic modulus, we also measure the elasticity. In order to avoid any confusion with the total energy, for which we also use the symbol E, we will use G_0 for the elasticity in the rest of this thesis, as this is the property which we measure.

The elasticity of the PEGDA posts is dependent on the size and concentration of the PEGDA monomers. When PEGDA polymerizes, it forms starlike polymers, arranged in a fractal network, illustrated in figure 2.6. This fractal network results in voids with a length scale larger than the radius of the stars, with a characteristic length scale ζ. This structure is what leads the elasticity of the crosslinked PEGDA to be strongly dependent on the length and volume fraction of the polymer used [21]. The elasticity is expected to increase with increasing polymer fraction. This is expected to be due to the crosslinking density in the system increasing with polymer fraction, thus forming a more close-packed, more difficult to deform particle. The elasticity is expected to decrease with increasing polymer length. This is expected to be due to the voids in the fractal structure. When the polymer is longer, this will result in larger voids and thus an easier to deform particle.

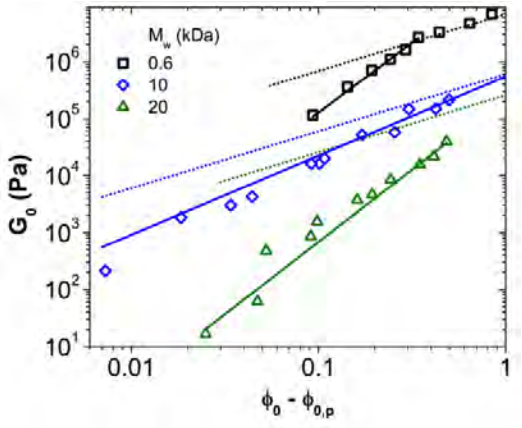

Fig. 2.7: Influence of PEGDA length and concentration on the shear elastic modulus G_0 as a function of volume fraction before mixing ϕ_0 minus the percolation threshold $\phi_{0,\mathrm{p}}$ (the lowest volume fraction for which crosslinking can occur). Image reproduced from [21].

Figure 2.7 shows a plot of experimental data from literature, where the influence of PEGDA length and concentration on elasticity were measured [21]. Note that in this case not ϕ is plotted as a measure of concentration, but $\phi_0 - \phi_{0,\mathrm{p}}$. Here, ϕ_0 is also a volume fraction, but it is the volume fraction before mixing. In other words, the volume of the solid PEGDA divided by the total volume after mixing. In general, ϕ is about ten times larger than ϕ_0. $\phi_{0,\mathrm{p}}$ is the percolation threshold, or the minimum volume fraction for which polymerization takes place. This value is on the order of 0.01 for the polymers shown. The experimental data shows the same relations as before: the elasticity increases with decreasing polymer length and increases with increasing polymer volume fraction.

2.2.3 Combining conformation change and binding energy

We have defined the two energies competing in the system: the depletion interaction and the elastic energy. The sum of these gives the total energy potential as a function of distance, which is plotted for

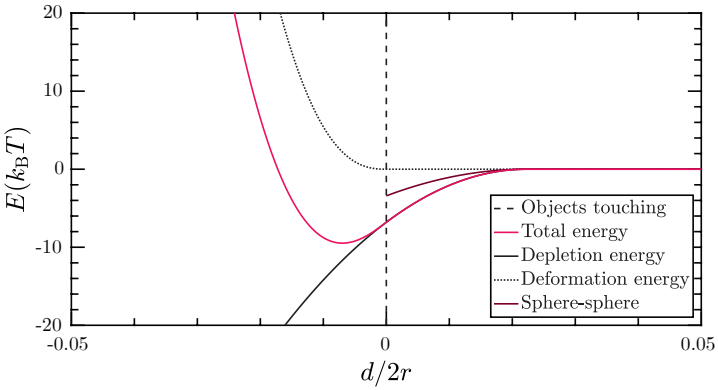

Fig. 2.8: Graph showing the depletion energy (black), the deformation energy (dotted) and the sum of those two, the total energy for sphere-wall interactions (pink) and sphere-sphere interactions (purple) for typical values. At $d/2r = 0$, the objects are touching (dashed line), at $d/2r = -0.05$, 5% of the particle is inside the wall.

typical values in figure 2.8. This plot shows both competing energies and the sum of the two, plus the depletion energy for two rigid polystyrene particles. It is obvious that the energy minimum for the particles interacting is much less deep than the energy minimum for the interaction between a particle and the wall. This means that it is more likely that the particles will interact with the wall than with each other.

The shape of this energy potential, of which the depth of the energy well is of particular interest, depends strongly on the various parameters in the system: elasticity of the post (G_0), radius of gyration of the depletant (R_g), volume fraction of the depletant (ϕ) and radius (r) of the particle, as shown in figure 2.9.

The energy minimum becomes deeper when the elasticity of the post gets smaller, which was to be expected, as the energy required for deformation becomes smaller with decreasing elasticity. The energy minimum also becomes deeper with increasing depletant concentration and particle size, which was also to be expected, as with bigger particles or more depletant, the depletion interaction will get stronger.

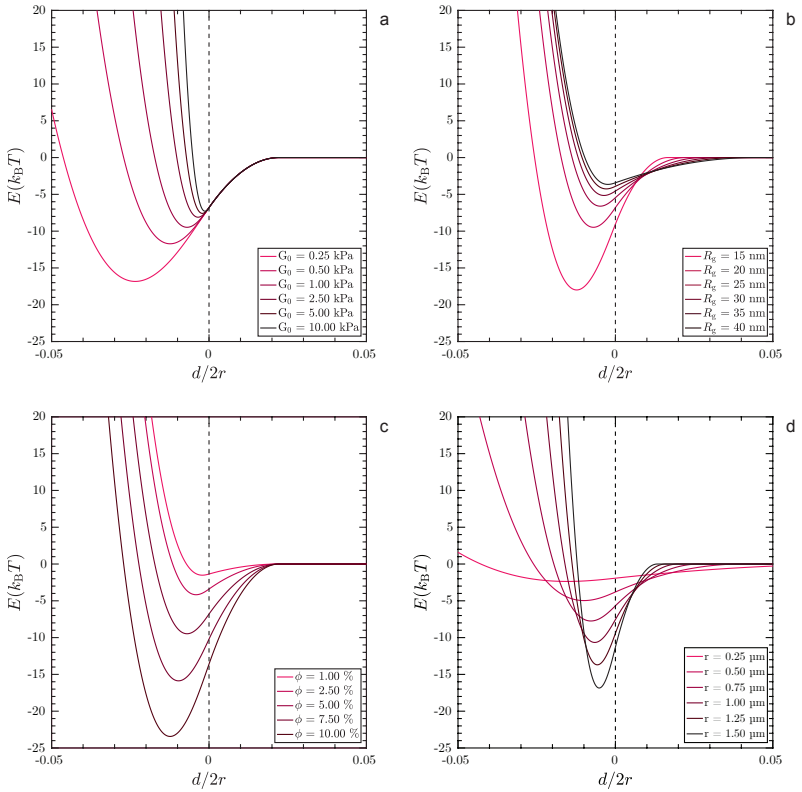

Fig. 2.9: Plots showing the relation between various parameters and the energy landscape, with (a) elasticity, (b) radius of gyration of the depletant, (c) volume fraction of depletant and (d) radius of the particle.
Typical values for the variables are: $G_0 = 1\,\mathrm{kPa}$, $R_\mathrm{g} = 20\,\mathrm{nm}$, $\phi = 5\,\%$ and $r = 0.9\,\mu\mathrm{m}$. The codes for calculating and plotting these graphs can be found in appendix B.

The energy minimum becomes deeper with decreasing radius of gyration. This makes sense when you think about how the concentration is defined. In figure 2.9b, ϕ is kept constant. With smaller depletant size, there will be more depletant particles per volume at the same ϕ. Since the depletion interaction is an entropic effect, it will increase with the amount of particles present in the system. Effectively, decreasing the depletant size has therefore the same effect as increasing the concentration of depletant. This effect is then much stronger than the overlap volume becoming slightly smaller and the depth of the energy minimum increases.

2.2.4 From energy potential to escape time

It is not possible to measure the depth of the energy potential directly. However, we can measure the escape time of the particles. The particle getting into an energy minimum constitutes a binding event. If the energy minimum is not too deep, the particle can also get out of this energy minimum again, constituting an unbinding event. We call the time required to observe an unbinding event the *escape time*, which can be calculated via numerical integration with equation 2.11, using Kraamer's method [22]

$$\tau = \frac{1}{D_0} \int_a^c \mathrm{e}^{-\beta E(d)} \mathrm{d}d \int_b^e \mathrm{e}^{\beta E(d)} \mathrm{d}d \tag{2.11}$$

where D_0 is the diffusion coefficient of the particles in the medium as calculated by the Stokes-Einstein equation, β the inverse of the thermal energy $(k_\mathrm{B}T)^{-1}$ and $E(d)$ the energy potential as a function of distance. Notice that $E(d)$ is negative in the first integral and positive in the second integral.

Figure 2.10 illustrates the boundaries of both integrals. The first integral goes from a to c, which are the points where $E = 0$. This integral gives the probability of the particle diffusing through the energy well. The second integral goes from b to e, which defines the region between the energy minimum and the particle being completely escaped. This integral gives the probability of the particle being released.

Of course, the particle is completely escaped for all values where $d > c$. However, the entire region ac is of the order of magnitude of 100 nm, which is less than one pixel for the optical microscope we use.

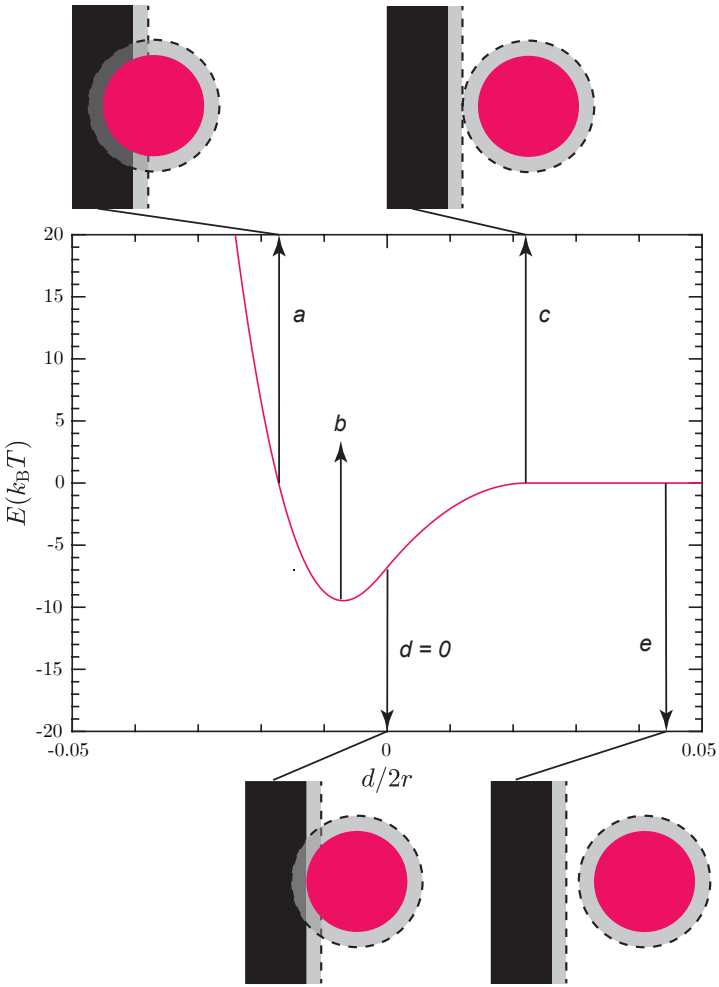

Fig. 2.10: The same energy as plotted in figure 2.8, but with the integration boundaries a (end of energy well), c (start of energy well), b (energy minimum) and e (particle escaped) indicated.

This is why the region ce is added: the distance a particle has to diffuse before it is visible that the particle has escaped. The value for e needs to be chosen as close to c as the resolution of the microscope will allow. In our case, this is about 400 nm, leading to an added diffusion time of about 3 s for typical values.

The escape time is governed by the depth of the energy minimum. Therefore, it is dependent on the same variables as the energy potential: elasticity of the post, radius of gyration of the depletant, volume fraction of the depletant and radius of the particles. The dependence of the escape time on these variables is shown in figure 2.11 for both the interactions of the particles with the deformable wall and for the particles with each other.

These plots confirm the relations seen in figure 2.9 for the interaction between particle and wall. The escape time decreases with increasing elasticity and depletant size, and increases with depletant concentration and particle size. For elasticity, radius of gyration and concentration of depletant the graph goes to a nonzero minimum value. This makes sense, as the particle has to diffuse from b to e, which will cost time, even if there is no interaction whatsoever with the wall. Notice how steep these curves are: the system is extremely sensitive to small changes in parameters.

Furthermore, these graphs show that the escape time of the particles that interact with each other is quite small, on the order of 3 s, which is the same as the diffusion time. Therefore, if the variables are chosen well, the interactions between the particles should be negligible.

The presented theory can provide with insights into realizing colloidal allostery. It shows that the binding affinity of the particles to the post could be tuned with post elasticity, thus providing with a substrate that can exist in multiple states, and that this energy could be measured via the escape time. In the next chapters, first steps are taken to verify this theoretical model experimentally.

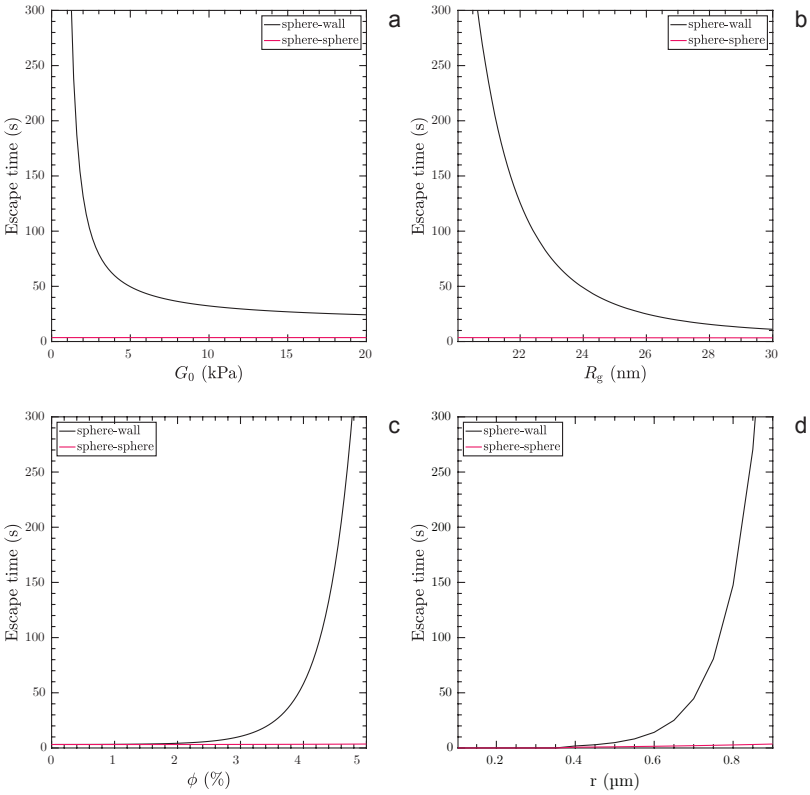

Fig. 2.11: Plots showing the relation between various parameters and the escape time, with (a) elasticity, (b) radius of gyration of the depletant, (c) volume fraction of depletant and (d) radius of the particle.
Typical values for the variables are: $G_0 = 1\,\mathrm{kPa}$, $R_\mathrm{g} = 20\,\mathrm{nm}$, $\phi = 5\,\%$ and $r = 0.9\,\mu\mathrm{m}$. The codes for calculating and plotting these graphs can be found in appendix B.

3. MATERIALS AND METHODS

In order to verify the theory developed in chapter 2, experiments were performed. In this chapter, we discuss the materials and methods used for these experiments. First, a list with materials is provided (section 3.1). The components of the system; the polystyrene particles (section 3.2), the microfluidic devices (section 3.3) and the PEGDA posts (sections 3.4), are discussed separately. Then the components are put together to perform and analyze depletion experiments, which is discussed section 3.5.

3.1 Materials

An overview of all materials used, as well as their abbreviations, can be found in table 3.1. All chemicals were used as received. The water used throughout this thesis was purified using a Milli-Q water purification system.

3.2 Synthesis of the polystyrene particles

3.2.1 Synthesis of the linear polystyrene particles (LPS)

Polystyrene particles where synthesized using standard emulsion polymerisation described in literature [23]. A water phase was prepared by dissolving 5.0 g PVP in 14 mL of water. An oil phase was prepared by dissolving 0.136 g AIBN in 10 mL styrene. 126 mL ethanol was added into a round bottom flask of 200 mL and both phases were added. The flask was closed with a stopper with a long glass rod attached, and sealed. The flask was then immersed in an oil bath of 75 °C at an axis of rotation of about 60°. Polymerization was carried out for 20 h while rotating at 60 rpm. Particles were washed twice with ethanol for 15 min

Tab. 3.1: Overview of used materials

Chemical	Abbreviation	Purity	Supplier
2-Hydroxy-2-methylpropiophenone	Darocur	97%	Sigma Aldrich
3-(trimethoxysilyl) propyl methacrylate	TPM	–	Sigma Aldrich
Divinylbenzene	DVB	80%	Sigma Aldrich
Isopropanol	–	99.5%	Sigma Aldrich
Poly (ethylene glycol) Mw 2000	PEG	–	Sigma Aldrich
Poly (ethylene glycol) diacrylate Mw 700	PEGDA	–	Sigma Aldrich
Poly (ethylene glycol) diacrylate Mw 6000	PEGDA	–	Sigma Aldrich
Poly (vinyl alcohol) Mw 89.000 98.000	PVA	99+%	Sigma Aldrich
Poly (vinyl pyrrolidone) Mw 40.000	PVP	–	Sigma Aldrich
Rhodamine B	–	–	Sigma Aldrich
Sodium dodecyl sulfate	SDS	99+%	Sigma Aldrich
Styrene	–	–	Sigma Aldrich
Azobis(isobutyronitrile)	AIBN	98%	Acros Organics
Potassium Permanganate	$KMnO_4$	–	BDH Chemicals
Sylgard 184, silicone elastomer	PDMS	–	DOW
Sylgard 184, curing agent	–	–	DOW
Ethanol	EtOH	100%	Interchema
Dichloromethane	DCM	–	Merck
Sodium hydroxide	NaOH	–	Merck
Sodium chloride	NaCl	–	Merck
Hydroquinone	–	–	Riedel de Haen
2,2'-Azobis(2,4-dimethyl valeronitrile)	V-65	–	Wako chemicals

at 3000 rpm and three times with water for 30 min at 3000 rpm using a table top centrifuge. The solid content was then determined gravimetrically and adjusted to 10 wt% by adding water. Finally, particles were transferred into a Pyrex bottle for storage.

3.2.2 Crosslinking the linear polystyrene particles (CPS)

For the water phase, 6.5 mg hydroquinone was dissolved in an 5 mL 5 wt% aqueous PVA solution and 14.2 mL of water was added. For the oil phase 0.18 g V-65 was dissolved in 9.8 mL styrene and 0.2 mL DVB was added. 2 mL of the oil phase and 8 mL of the aqueous phase were added together in an elongated 20 mL glass vial and emulsified using an UltraTurrax at 8000 rpm for 5 min. A couple of mL of LPS were added to the swelling emulsion to obtain the desired swelling ratio. Typically, 5 mL was added to obtain a swelling ratio of 4. The mixtures were then flushed by inserting a needle with a nitrogen flow, ensuring a low flow to avoid spillage. The vial was then closed, sealed with parafilm and left on a roller table for 24 h. Afterwards, the vial was securely attached to a metal stirrer and immersed in an oil bath at 70 °C at an axis of rotation of 60°. The vial was left stirring at 100 rpm for 24 h. The dispersion was then washed five times with water for 15 min at 2000 rpm using a table top centrifuge. Solid content was measured gravimetrically and adjusted to 5 wt% by adding water. Finally, particles were transferred into an appropriately sized glass vial for storage.

3.2.3 Dyeing the crosslinked particles (CPSR)

A 12.5 $mg\,g^{-1}$ solution of SDS in water was prepared by dissolving 25 mg of SDS in 2 g of water. A 0.4 $mg\,g^{-1}$ (= 1 $mmol\,L^{-1}$) solution of Rhodamine B in DCM was prepared by dissolving 12 mg of Rhodamine B in 4 mL (≈ 5 g) of DCM. The dyeing mixture was then prepared by taking a 4 mL glass vial and adding 1 g of 0.4 $mg\,g^{-1}$ (= 1 $mmol\,L^{-1}$) Rhodamine B in DCM, 1 g of 5 wt% crosslinked polystyrene particles (CPS) and 2 g of 12.5 $mg\,g^{-1}$ SDS in water, resulting in a mixture of DCM : water as 1 : 3 with 0.1 $mg\,g^{-1}$ Rhodamine B, 12.5 $mg\,g^{-1}$ CPS and 5 $mg\,g^{-1}$ SDS. The vial was sealed with parafilm, put on the roller bank and left for 48 h. The mixture was then divided evenly over two 15 mL vials and a stirring bean was added to both vials. The mixture

was stirred at about 400 rpm inside a flow box with the caps off for 6 h to evaporate all DCM. The mixtures were then transferred to Eppendorf tubes and washed three times with water using a micro centrifuge at 2500 g for 5 min to remove excess SDS. Between each washing step, it was ensured that there were only two phases visible. If three phases were visible, washing was stopped and evaporating was continued to prevent aggregation. Finally, both dyeing mixtures were recombined in a 4 mL glass vial. Solid content was measured gravimetrically and a sample was diluted to an approximate concentration of 0.02 wt% to get the measuring concentration.

3.2.4 Characterization of the particles

The success of synthesis of the particles was determined by diluting a sample approximately 100 times, placing a droplet onto a cover slip and then looking at them using a Nikon TiE optical microscope, typically with a 10x objective. The success of the dyeing process was determined by switching to the RITC mode of the microscope and visually determining the sufficiency of the contrast between particles and background. Finally, transmission electron microscopy (TEM) pictures were taken with a Philips Technai10 electron microscope, typically operating at 100 kV, to determine particle size. The samples were prepared by drying a drop of diluted aqueous particle dispersion on top of polymer-coated copper grids.

3.3 Preparing the microfluidic devices

The process of preparing the microfluidic devices described below is illustrated in 3.1.

3.3.1 Preparing the chips

The PDMS mixture was prepared using the Sylgard 184 kit, containing both PDMS monomers and the curing agent. 35 g of PDMS monomer and 5 g of curing agent where added together inside a falcon tube. The mixture was stirred for 2 min using an overhead stirrer until completely opaque and then centrifuged for 15 min at 3500 rpm to get rid of bubbles.

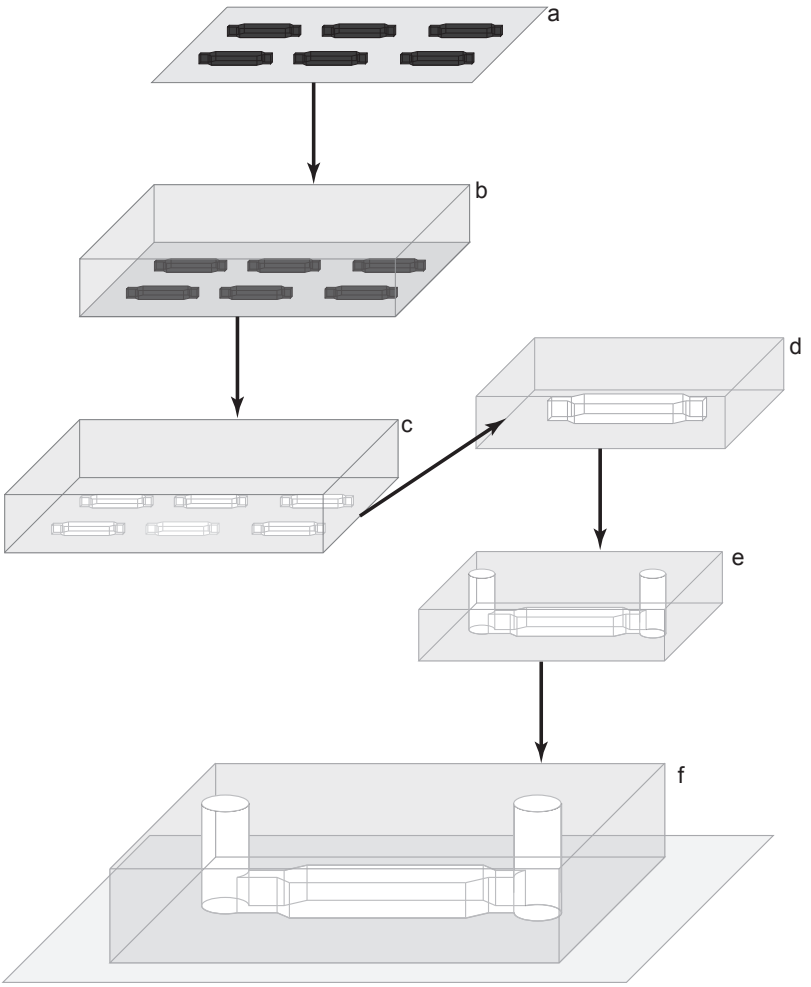

Fig. 3.1: Illustration showing how the microfluidic chips are prepared. Starting with a mold (a) over which PDMS is poured (b), which is removed after hardening (c). Then, individual chips are cut out (d), inlet and outlet are created (e) and the chip is fixed on a glass slide (f) obtaining the final device.

The chips were made using a previously manufactured mold, consisting of a silicone wafer with the negative of the channels on top of them. If the mold had been used 10 times, it was re-hydrophobized. To do this, 10 droplets of PFS were put into a glass vial. The vial was then put inside the desiccator on its side, together with the mold. This was then desiccated for 2 h.

The mold was cleaned with isopropanol and then dried under a nitrogen stream. The PDMS mixture was poured slowly over the mold. This was desiccated without the lid for 2 h to get rid of all the bubbles. The petri dish was closed and placed in the oven overnight at 65 °C. The mold was cut from the wafer carefully using a razor blade and put feature side up in a clean petri dish, which was placed on a black background. Scotch tape was placed along the channels on top of the features to protect them. Individual chips were then cut from the PDMS, while care was taken that they remained feature side up. The inlet and outlet were created by placing a ⌀1 mm biopsy punch orthogonal to the surface and pushing through the chip in one swift, straight motion. The plunger was used to remove the PDMS from the punch.

3.3.2 Preparing the glass slides

A 1 mol L^{-1} (40 mg g^{-1}) solution of NaOH in water was prepared by dissolving 20 g of NaOH in 500 mL of water. A falcon tube was filled with the NaOH solution and about 20 glass microscopy slides slides (22 mm × 50 mm #1.5) were immersed in it. The slides were left for 30 min, after which the NaOH was replaced with water and left for 5 min. The slides where then rinsed once more with water. If necessary, the slides were stored in water.

3.3.3 Assembling the devices

The microchips were cleaned by immersing them in EtOH inside falcon tubes and placing them into an ultrasonic bath for 5 min, after which they were rinsed with EtOH and water and dried under a nitrogen stream. When the humidity was high, this step was skipped to prevent the microchips not sticking to the glass slides. The glass slides were rinsed thoroughly with water, and then dried under a nitrogen stream.

The glass slide and the microchip were placed on a piece of aluminium foil. Both the slide and the microchip were cleaned for 5 s using a plasma gun. Care was taken to not use the plasma gun for more than 5 s to prevent damaging the device. The chip was picked up by its sides and placed on the glass slide, without pressing on it. The microfluidic devices were placed in a clean petri dish and put inside the oven for 2 h at 65 °C to eliminate any delamination.

3.3.4 Functionalizing the devices

A functionalization fluid of 25 mg mL^{-1} TPM in EtOH was prepared by dissolving 75 mg of TPM in 3 mL of EtOH. A 1 mol L^{-1} (40 mg g^{-1}) solution of NaOH in water was prepared by dissolving 20 g of NaOH in 500 mL of water. It was made sure that the devices had completely cooled down to prevent leaking. An inlet and outlet were created by inserting ⌀1 mm Luer stubs. The devices were rinsed with 300 µL of water and then twice with air using a 1 mL syringe, after which they were filled with the 1 mol L^{-1} NaOH solution and left for an hour. The devices were then rinsed with 300 µL of water and twice with air using another 1 mL syringe. The devices were filled with acrylate solution and left for 30 min, after which they were rinsed with 300 µL of EtOH and then twice with air using another 1 mL syringe. The devices were then put into the oven at 65 °C overnight.

3.4 Synthesizing the posts inside the channel

3.4.1 Preparing hard post mixture

A glass vial was wrapped in aluminium foil to prevent any light pollution. 990 µL of PEGDA 700 and 10 µL of Darocur were added to the vial and the mixture was homogenized by placing it inside an ultrasonic bath for 10 min. The vial was then placed into a light-sealed container inside a fridge at 4 °C for storage.

3.4.2 Preparing soft post mixture

A glass vial was wrapped in aluminium foil to prevent any light pollution. The desired amounts of PEGDA 6000 and PEG 2000 were

weighed and water was added to a weight of 990 mg. Typically, concentrations of 20 % PEG 2000 and 2 % to 8 % PEGDA 6000 were used. The vial was placed on the rollerbank for 10 min or until the PEGDA 6000 and PEG 2000 had completely dissolved. Then, 10 µL of Darocur was added to the vial and the mixture was homogenized by placing it inside an ultrasonic bath for 10 min. The vial was then placed into a light-sealed container inside the fridge at 4 °C for storage.

3.4.3 Synthesizing the posts

The process used for the synthesis of the posts described below is schematically illustrated in figure 3.2.

The post mixtures were taken out of the fridge, brought to room temperature and homogenized by placing them inside the ultrasonic bath for 10 min. A round 1000 µm photomask (resulting in $\approx$ ⌀40 µm posts) was placed inside the field stop of the UV lamp of a Nikon TiE microscope. A microfluidic device was taken out of storage and checked for delamination or pollution. If the channel was polluted, the channel was put into a falcon tube, immersed in EtOH and placed inside an ultrasonic bath for 45 min. The EtOH was then replaced by water and the tube was placed back into the ultrasonic bath for another 45 min, after which the device was dried under a nitrogen stream. An inlet and outlet were created by inserting two ⌀1 mm Luer stubs. At 40x magnification, the UV lamp was turned on once to determine where the post was going to be. The channel was filled with hard post mixture using a pressure gauge, typically at a pressure of 1.0 psi (0.07 bar). Small posts were made by illuminating with UV light through the photo mask at 40x magnification, typically for 0.5 s, creating cylindrical posts that are fixed to the bottom of the channel, as illustrated in figure 3.2. The 1000 µm photomask was replaced by a 2300 µm photo mask to achieve the large posts ($\approx$ ⌀100 µm). The desired number of hard posts were created around the small posts, again by illuminating with UV light through the photomask at 40x magnification, typically for 0.5 s. The channel was rinsed with 30 µL of water, typically at a pressure of 2.5 psi (0.17 bar), and filled with soft post mixture, typically at a pressure of 1.0 psi (0.07 bar). The desired number of soft posts were created around the small hard posts, by illuminating with UV light through the photomask at 40x magnification, typically for 2 s.

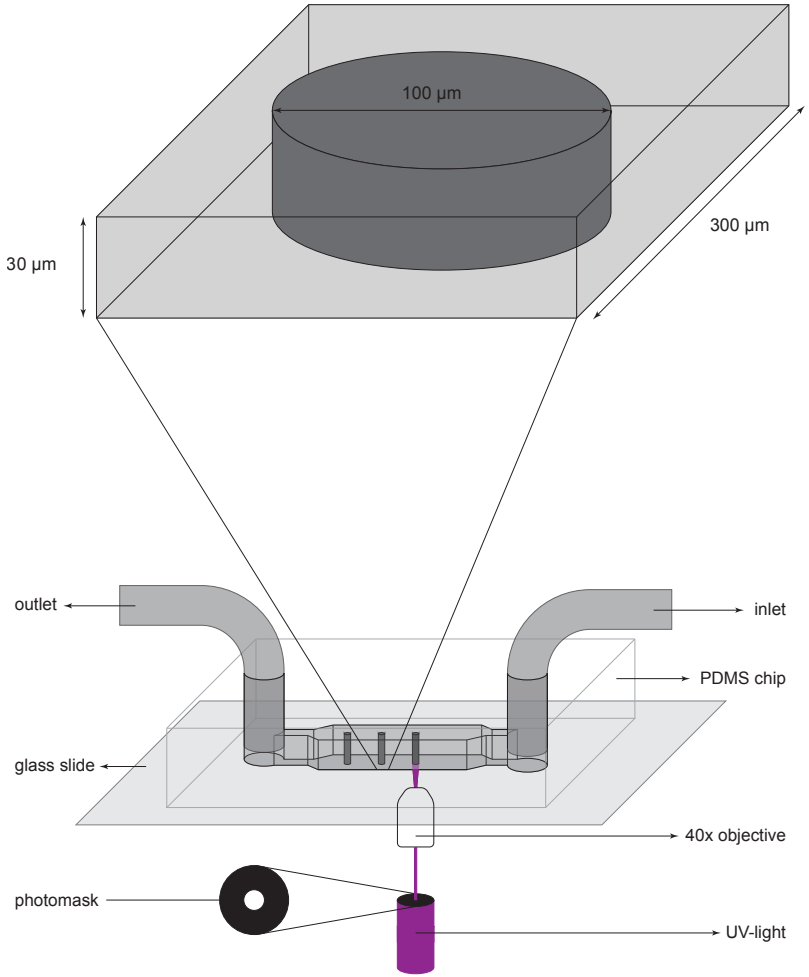

Fig. 3.2: Illustration of the synthesis process of the posts. The microfluidic channel is filled with PEGDA mixture and is illuminated with UV-light through a photomask, thus creating a cylindrical post that is fixed to the bottom of the channel. The cutout shows a more to scale image of the post that is created inside the channel.

The channel was then preferably immediately used for experiments. If storage proved to be necessary, the channel was stored inside a falcon tube, immersed in water.

3.4.4 Rheology

Rheology of PEGDA mixtures was measured using a Discovery HR-2 Hybrid Rheometer and a UV lamp with an intensity of about 100 mW cm^{-2} at a distance of 5 cm. Measurements were taken *in situ* by adding monomer mixture, measuring for 1 min, then illuminating with UV light for 5 s and then measuring again for 1 min.

3.5 Performing depletion experiments

3.5.1 Preparing a particle mixture

A stock solution of 27.25 g L^{-1} dextran in water ($\phi = 1$) was prepared by dissolving 545 mg dextran in 20 mL of water. The stock solution was diluted to 5 times the desired concentration. A stock solution of 50 mmol L^{-1} NaCl in water was prepared by dissolving 90 mg NaCl in 30 mL water, which was diluted to 5 mmol L^{-1}. The experimental mixture was prepared inside a small Eppendorf tube by adding together 20 µL of 5 mmol L^{-1} NaCl solution, 20 µL of depletant solution and 60 µL of diluted CPSR-dispersion. This mixture was homogenized by placing it inside an ultrasonic bath for about 5 min.

3.5.2 Performing an escape time experiment

The microchip with posts was dried completely under 2.5 psi (0.17 bar) and filled with the experimental mixture at 0.5 psi (0.035 bar), after which the inlet and outlet were sealed with scotch tape. A measuring spot, containing both a hard post and a soft post, was selected with the 40x objective and a single picture was taken in bright field mode for determining the post positions as well as seeing the starting conditions. A ND acquisition was done in RITC with a frame rate of 1 fps to 2 fps, typically for 1 h. The shutter was closed in between pictures to reduce photo bleaching. After the experiment, another single picture was taken in bright field. The channel was usually discarded after use.

3.5.3 Analyzing an escape time experiment

The method for analysis described below is schematically illustrated in figure 3.3. The MATLAB codes referred to in this section can be found in appendix C.

The BF picture of the posts was loaded in ImageJ and the positions and radii of the posts were determined by drawing a circle and using the measuring tool, which were then saved in a .txt file. The ND acquisition was loaded in ImageJ, 500 frames at a time, converted to 8 bit and saved as .tif in consecutive files. These .tif files, were plugged into a MATLAB tracking script. The tracking and post positions were then combined to obtain tracks relative to the center of the post. Escape times were determined by counting the amount of consecutive frames a track would be below the first dotted line (e). Escape times and standard deviations were determined for the hard post and the soft post. Diffusion time was also determined as a control.

3.5.4 Performing a sticking experiment

The microchip with posts was dried completely with air, using a pressure of 2.5 psi (0.17 bar) and then filled with the experimental mixture at 0.5 psi (0.035 bar). The inlet and outlet were sealed with scotch tape. Using a Nikon TiE microscope with a 40x objective, positions of measuring spots, of which there were typically between 5 and 10, were determined. Then, an ND acquisition was done simultaneously for each measuring spot, in both RITC and BF, with a frame rate of 1 frame/min, typically for 1 hour. The shutter was closed in between pictures to reduce photo bleaching. The channel was usually discarded after use.

3.5.5 Analyzing a sticking experiment

The sticking experiments were analyzed by loading the ND-acquisitions one measuring point after another in ImageJ and counting the amount of particles stuck at t = 0 min and at t = 60 min by hand, for each measuring point. The entire ND-acquisition was always inspected to check for any unexpected behavior. MATLAB was then used to obtain a graph of the amount of stuck particles at t = 60 min versus the desired variable.

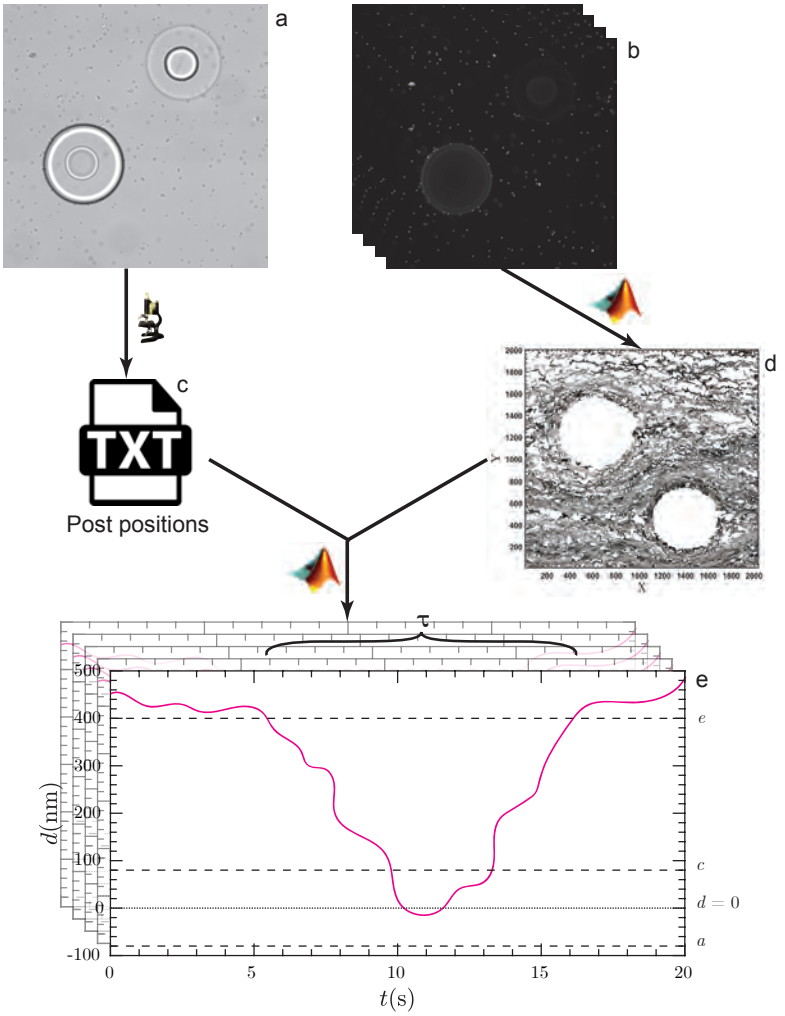

Fig. 3.3: Illustration of the analysis of the escape time. Post postitions are determined using a BF picture (a) using ImageJ, particle tracking is performed on the RITC ND-acquisition (b) using MATLAB. These (c, d) are then combined in MATLAB to obtain relative tracks (e), which are used to determine the escape time τ.

4. RESULTS AND DISCUSSION, PART 1: THE SEPARATE COMPONENTS

During this research, a lot of insight was gained into the optimal ways of obtaining the separate components of the system. In this chapter, we will discuss these separate components: the polystyrene particles (section 4.1), the microfluidic devices (section 4.2) and the PEGDA posts (section 4.3).

4.1 Synthesis of the polystyrene particles

Polystyrene particles dyed with Rhodamine and sterically stabilized by PVP were synthesized according to the methods described in methods (section 3.2). Several different variations on the synthesis method were tried, to establish the best route for synthesis. These variations will be described further in the rest of this section.

Finally, CPSR-13 (crosslinked polystyrene particles dyed with rhodamine batch 13) was chosen as the most suitable for experiments. Using TEM, the approximate size distribution of an earlier batch of particles (CPSR-04) had been established. Figure 4.1b shows a representative TEM picture of the particles and figure 4.1a shows the size distribution. The diameter was established to be 1890 nm, with a standard deviation of 71 nm. This number was confirmed for batch 13 by using dynamic light scattering (DLS).

Figure 4.1c and d show microscopy pictures of the particles that were used in the final experiments, respectively in bright field (BF) and fluorescence (RITC) mode. The particles are well visible, well dispersed and provide a good contrast against the background in RITC mode.

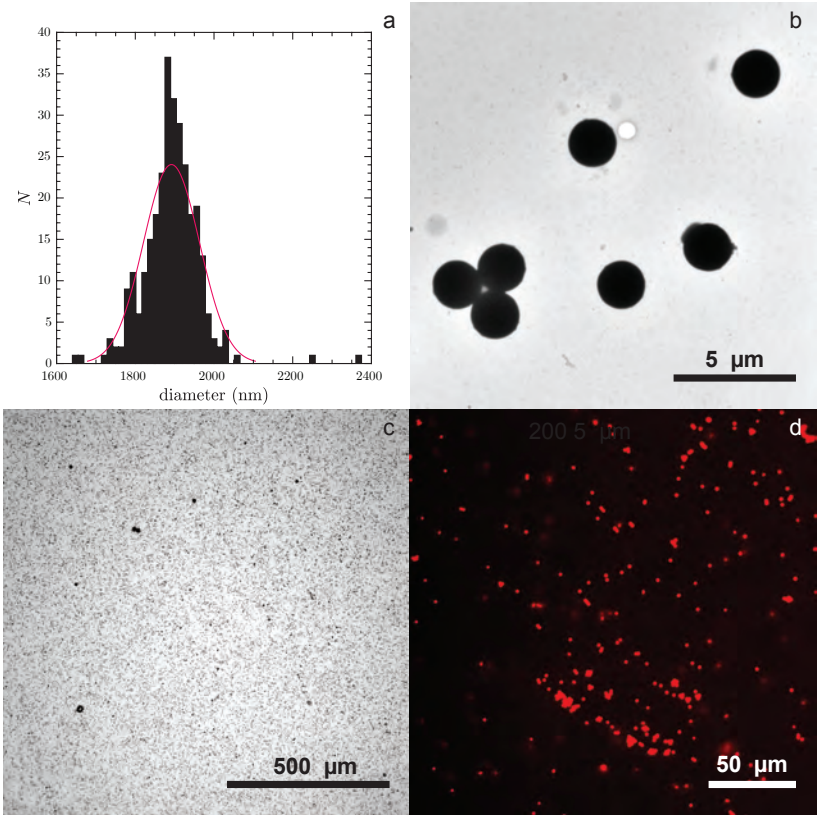

Fig. 4.1: Figure showing the properties of the particles used with (a) distribution of sizes measured on the similar particles, (b) a TEM picture of the similar particles, (c) a picture of the particles used taken with a 10x objective in BF mode and (d) a picture of the particles used taken with a 40x objective in RITC mode.

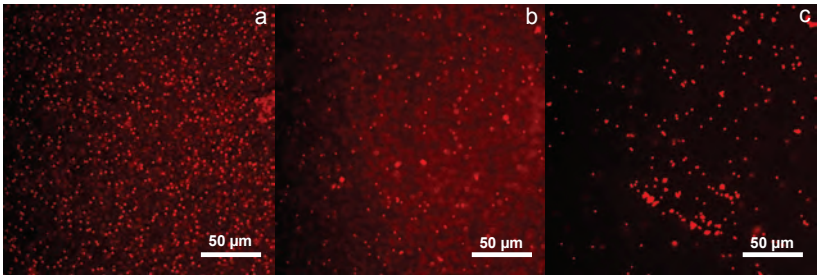

Fig. 4.2: Optical microscopy pictures taken of various particles in RITC mode where (a) the particles where dyed during cross-linking, (b) the particles were dyed for 24 hours after they had been cross-linked and (c) the particles were dyed for 48 hours after they had been cross-linked.

4.1.1 Variation 1: crosslinking with PVP instead of PVA

It was tried to substitute the PVA in the aqueous phase of the crosslinking mixture with PVP, since PVP was already present in the system. However, this resulted in all the polystyrene particles aggregating. This could be due to the molar mass of the PVP used being twice as small as the molar mass of the PVA. The PVP might therefore not be able to stabilize the crosslinking emulsion enough to prevent uncontrolled swelling. This variation was dismissed and not further investigated.

4.1.2 Variation 2: dyeing while crosslinking and shorter dyeing times

It was tried to dye the polystyrene particles during crosslinking by adding Rhodamine B to the oil phase of the crosslinking emulsion in an effort to make the synthesis procedure more efficient. It was also tried to dye the polystyrene particles for only 24 hours instead of 48 hours, to shorten the synthesis time.

In figure 4.2 optical microscopy pictures, taken in RITC mode, are shown of the dyeing while crosslinking trial, as well as dyeing in a separate step for respectively 24 and 48 hours. The dyeing while crosslinking, as well as the shorter dyeing time, did result in dyed particles. However, the contrast is much less than when the particles are dyed for 48 hours. Therefore, these variations were also dismissed.

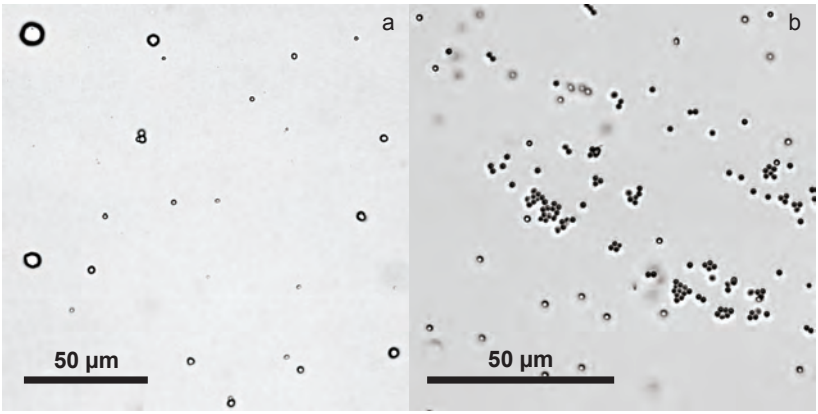

Fig. 4.3: Optical microscopy pictures of cross-linked and dyed polystyrene particles, taken in BF mode where in (a) there was no SDS used in the dyeing process and in (b) $5\,\mathrm{mg\,mL^{-1}}$ SDS was added to the dyeing mixture.

4.1.3 Variation 3: dyeing without SDS

It was also tried to dye the particles without the SDS present. If successful, this could ease the washing of the particles a lot, since there would be no excess SDS to wash away. However, SDS proved to be necessary to the dyeing process. In figure 4.3, optical microscopy pictures are shown of particles dyed with and without SDS present. Without SDS present, the particles aggregate and melt together. SDS is probably necessary to stabilize the emulsion of DCM in water that is the dyeing mixture. Without the SDS, the dyeing mixture phase separates, resulting in uncontrolled swelling of the particles. This variation was therefore also dismissed.

4.1.4 Variation 4: different evaporation methods

The DCM needs to be evaporated from the dyeing mixture before washing. When the DCM is not completely evaporated, this will lead to three phases being visible after centrifuging, which in turn leads to the particles aggregating.

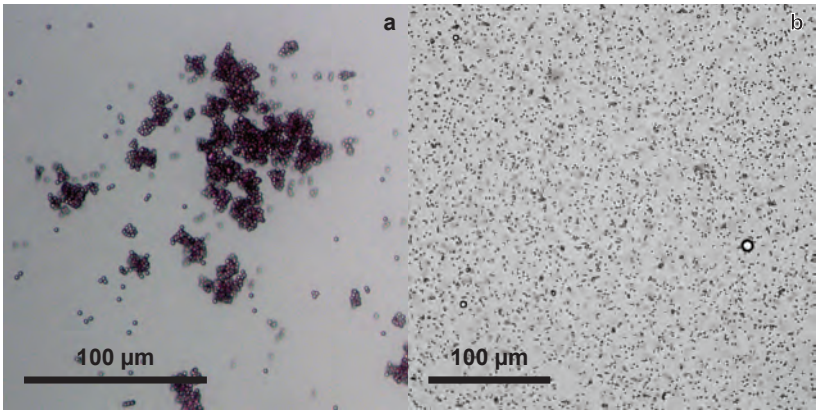

Fig. 4.4: Optical microscopy pictures of two crosslinked and dyed particle samples, where (a) was evaporated in a 4 mL vial without stirring for 6 h and then washed and (b) was evaporated in a 15 mL vial with a stirring bar for 6 h and then washed.

Figure 4.4 illustrates the difference between a sample that did aggregate during washing and a sample that did not. The evaporation time should not be too long, as evaporating takes place without the vial being covered and therefore, the longer the evaporation time, the more dust can get in. Furthermore, as there is an open vial with DCM present, heating as well as letting it sit overnight would not be advisable. It proved very successful to divide the dying mixture evenly over two 15 mL vials and then letting them evaporate for 6 h inside a flow box to prevent dust. This variation was therefore incorporated into the standard protocol as written in section 4.1.

4.2 The microfluidic devices

Microfluidic devices were prepared and successfully functionalized with TPM to enhance the binding of PEGDA posts to the glass of the channel. A lot of insight in practical matters was obtained while working with these devices. This section discusses these practical insights.

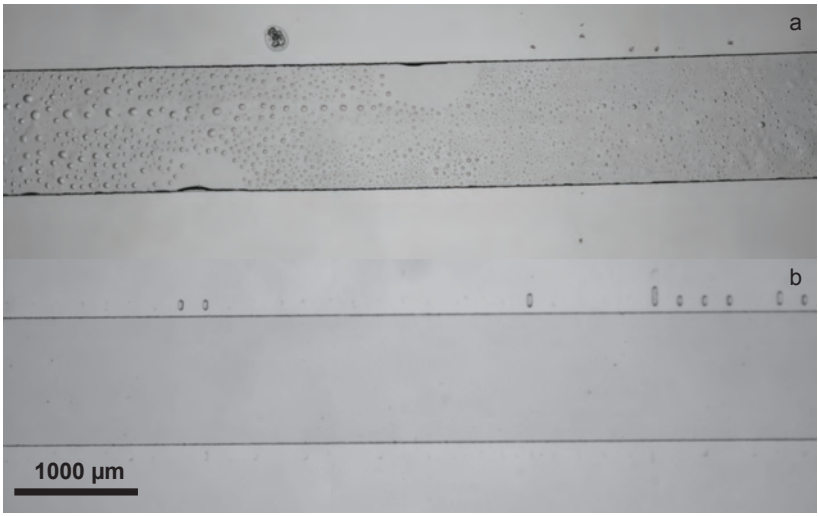

Fig. 4.5: Optical microscopy pictures of a channel where (a) the channel was functionalized using a high concentration of TPM in water and ethanol and (b) the channel was functionalized with a low concentration of TPM in only ethanol.

4.2.1 Bubbles inside the channel

Figure 4.5 shows two channels directly out of storage. In the channel in figure 4.5a, bubbles did arise. The bubbles could not be removed by water, ethanol or heat. After every synthesis step, the channel was inspected under the optical microscope to verify what was causing the bubbles. It was found that the TPM caused them. It could be that what looks like bubbles in the channels, are actually TPM precipitates. The bubbles can be prevented by dissolving the TPM in EtOH only, or using a lower concentration.

4.2.2 Dusty channels

It was found to be very important that the devices are created in an environment that is as dust-free as possible. This means working inside a fully functional flow box, with gloves, and always making sure that

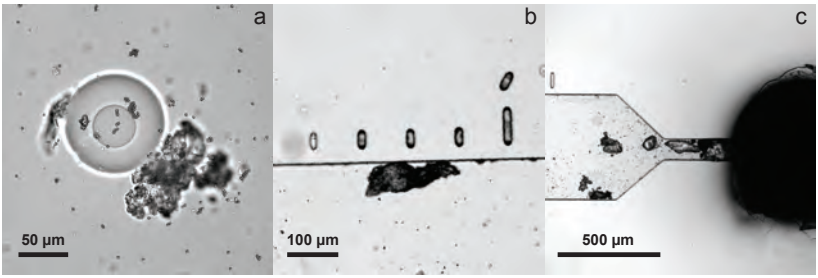

Fig. 4.6: Optical microscopy pictures of situations where dust got into a channel with (a) dust being stuck to a post, (b) a dust particle on the side of a channel and (c) dust at the inlet, blocking it.

all fluids that go inside the channel are freshly prepared. The petri dish with the channels should always be closed when outside the flow box and spend as little time outside as possible. If these measures are not taken, dust will get into the channel, leading to blocked channels and ruined experiments, as illustrated in figure 4.6.

4.2.3 Leaky channels

Two types of leakage did arise when using the channels: leakage from the edges of the microchip and leakage from the inlet and outlet. Leaking around the edges was caused by delamination. It was found that the step of washing the microchannel can be skipped when the weather is very humid to prevent delamination. Furthermore, assembling the devices, the chips should never be pressed on. This is probably due to the devices being a little elastic, and springing back after they are pressed on, causing delamination. It was found that small delaminations would usually dissapear after about 2 h in the oven at 65 °C.

The leakage from the inlet and the outlet could be due to the biopsy punch used: these punches are not made to be exactly 1 mm in diameter. Furthermore, it was found that this type leakage could largely be prevented by ensuring that the devices have fully cooled down after they have spent time in the oven. This might be due to the PDMS still being soft when it is hot and therefore not giving enough resistance to the Luer stubs, causing fluid to be able to escape.

4.3 The PEGDA posts

In this section, the synthesis of the posts used is discussed. The recipe for successful mixtures is discussed and practical issues with making the posts inside the channel are treated.

4.3.1 Successful PEGDA recipes

For the experiments, it was necessary that both a mixture that would create a very hard post as well as a mixture that would create a very soft post could be prepared. For the hard posts, a mixture of PEGDA 700 with 1 wt% Darocur was used and proved successful, with visible crosslinking at an exposure of 5 ms.

With the soft posts, however, crosslinking was often not visible, or different throughout the channel. It was postulated that this was because the Darocur would not dissolve completely and therefore never being homogeneously distributed throughout the mixture. Different amounts of PEG 2000 were added to try and dissolve the Darocur. It was shown that Darocur would dissolve completely at a PEG concentration of 20 wt%. By ultrasonication, it was ensured that the mixture was always homogeneous. This way, soft posts could be created consistently from a PEGDA 6000 concentration of 4 wt% ($\phi = 0.55$) or higher, with an exposure time of 2 s.

4.3.2 Estimating the elasticities of the posts

Rheology has been used to estimate the elasticity of the different post mixtures, as well as determining whether adding the PEG 2000 had any influence on the elasticity of the posts. Both G' and G'' were measured, but G'' was found to be negligible. Therefore, G' is interchangeable with G_0. Figure 4.7a shows the graphs directly from the rheometer. Several concentrations of PEGDA 6000 where measured, all mixtures contained 20 wt% PEG 2000. The regions where there was no illumination, during illumination and after illumination are easily distinguishable. Complete cross-linking is assumed. This figure shows the extreme variation in the elasticity of the posts, ranging from barely distinguishable from uncross-linked to several MPa, depending on the concentration and length of PEGDA used.

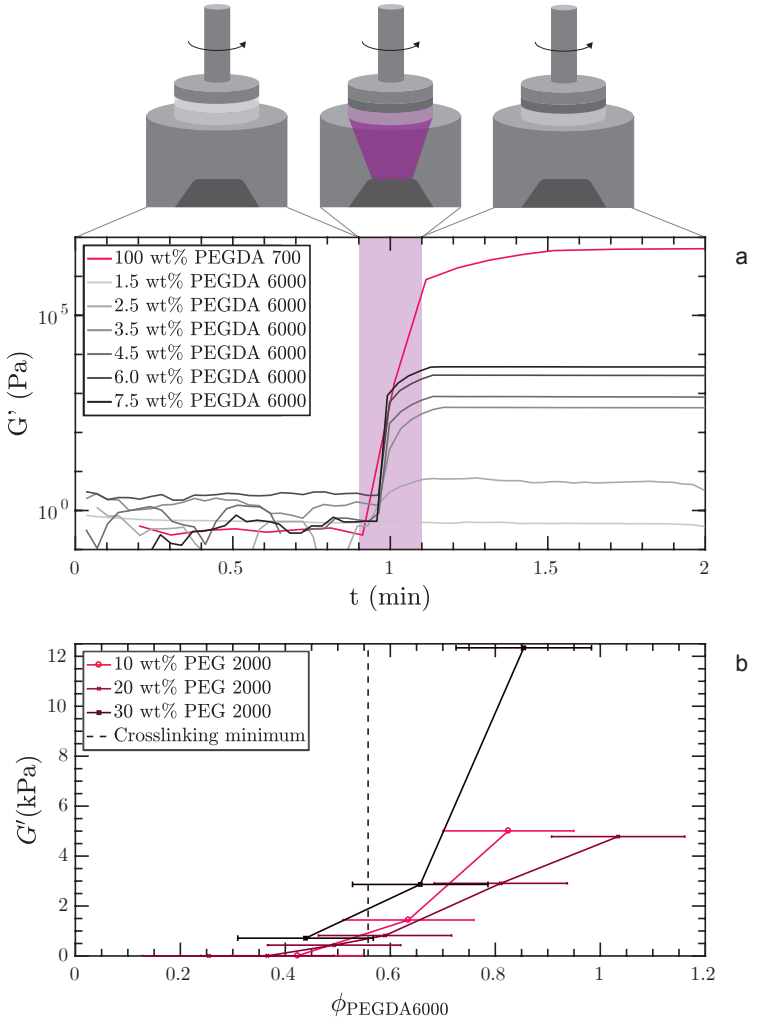

Fig. 4.7: Elasticities of PEGDA mixtures where (a) shows the shear modulus as a function of time. All PEGDA 6000 mixes contained 20 wt% PEGDA 2000. The region where the mixture is illuminated with UV-light is coloured purple. Figure (b) shows the elasticity as a function of PEGDA 6000 volume fraction.

Figure 4.7b shows how the concentration of PEGDA 6000, as well as the concentration of PEG 2000, influences the elasticity of the crosslinking mixtures. It is clear that the elasticity of the post is sensitive to the concentration of PEGDA used. However, the concentration of PEG does not influence the elasticity of the posts, when taking the horizontal error bars into account. This could be due to the relative sizes of PEG 2000 and PEGDA 6000. PEG 2000 has a R_g of approximately 1.8 nm, wheras the R_g of PEG 6000 is 3.2 nm [24]. Assuming the radius of gyration of PEGDA 6000 to be roughly equal to PEG 6000, it means that the PEG 2000 might not be big enough to interfere with the characteristic length and thus the elasticity of the gel that is formed.

When the PEGDA mixes were put inside a channel, visible crosslinking was achieved when concentrations upwards of 4 wt% were used. This is indicated with the dashed line in figure 4.7b. This means that it is possible to tune the elasticity of the PEGDA posts over four orders of magnitude.

Rheology is not the most reliable method for measuring exact elasticities of the posts. Rheology is very dependent on the exact measuring method used and results can therefore differ up to an order of magnitude, just by changing the method of measuring. Furthermore, we can assume complete cross-linking when measuring and it is unclear if complete cross-linking can be assumed inside the channels. Finally, this value is still in bulk and not on the micro scale. These measurements do, however, provide with a general idea, which shows that the elasticity can be tuned over several orders of magnitude and that the elasticity is extremely sensitive to the PEGDA concentration and not to the PEG concentration added. The values we find for the bulk elasticity of the soft posts are of the same order of magnitude as the values found in literature [21].

4.3.3 Synthesizing posts inside the channel

It is important to use the right focus when synthesizing posts. In figure 4.8a, a post that was made with correct focusing is shown, while in figure 4.8b, a post that was made when very unfocused is shown. Making the posts when the microscope is not correctly focused will lead to posts that are bigger, with fuzzier edges. Since the depth of focus of the microscope is on the order of microns, only a few micrometers

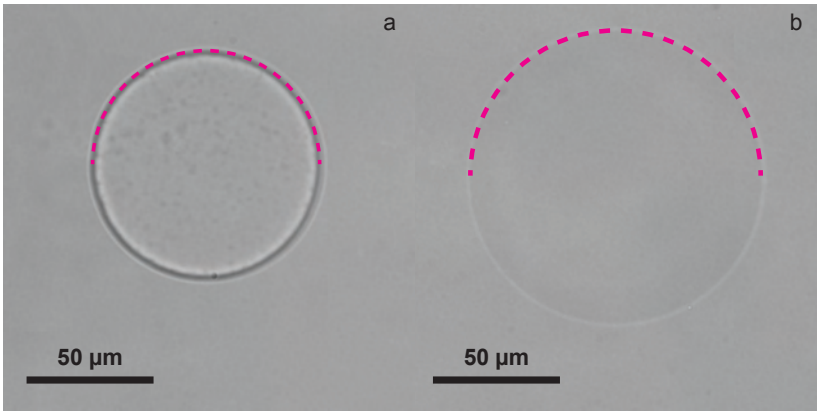

Fig. 4.8: Comparing optical microscopy pictures of two posts where in (a) the focusing was correct and in (b) the focusing was incorrect. The pink lines provide with an aid for distinguishing the edges of the posts.

off in focus will already lead to a noticeable difference in posts.

The focusing is a weak point of the method. Focusing is subjective and therefore not only different from scientist to scientist, but even different from experiment to experiment or post to post. Large focusing errors are usually quite obvious and therefore these posts can be taken out of analysis. Small focusing errors, however, can only be accounted for by doing the same experiment several times and averaging over the results, thus averaging out differences that can not be seen by eye. Furthermore, differences in focussing lead to differences in the exact shape of the post. The post is not completely straight, but a bit conical in shape, leading to the black border around the posts. The degree of conicity is also determined by the exact focal point used.

Exposure is another very important, but easier to control parameter. In figure 4.9, a post that was underexposed, correctly exposed and overexposed are shown next to each other. When the posts are under exposed, this can lead to fuzzy, unclear posts. This could mean that the post is not completely cross-linked, which leads to added difficulty in estimating the real elasticity of the post. When the post is overexposed, it can lead to a halo effect, probably due to the diffraction of

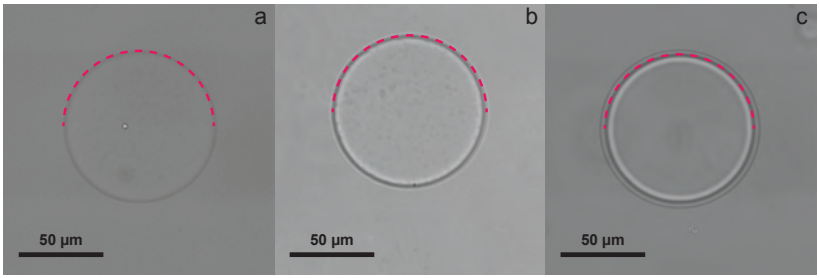

Fig. 4.9: Optical microscopy pictures of posts, where (a) was underexposed, (b) was correctly exposed and (c) was over-exposed. The pink lines provide with an aid for distinguishing the edges of the posts.

the UV light by the PDMS of the microchip. This also leads to added difficulty in estimating the real elasticity of the post, as it is unclear what the elasticity of the halo is.

Overexposing can be prevented both by exposing for a shorter time and exposing with a lower intensity. Both, however, could also lead to incomplete cross-linking. A method was found to prevent overexposure, while at the same time allowing for exposure times long enough that complete cross-linking could be assumed. It was found that there are no halo effects or fuzzy particles when the mixture was exposed several times for a short time, with a short waiting time in between the exposures.

4.3.4 Snowman posts and omelette posts

Even though the glass surface was functionalized with TPM, the soft posts proved to be prone to shifting and distorting. It was found out that this can be prevented by using a hard post to stabilize the soft post. In first instance, snowman posts were tried (figure 4.10a). These posts proved very effective in providing with stable posts, as well as ensuring that a hard post and soft post could be investigated at the same time. However, the snowman posts also lessen the surface exposed to the medium, leading to fewer events and worse statistics. Furthermore, the posts do not experience the exact same environment, since there will always be initial flow from one side.

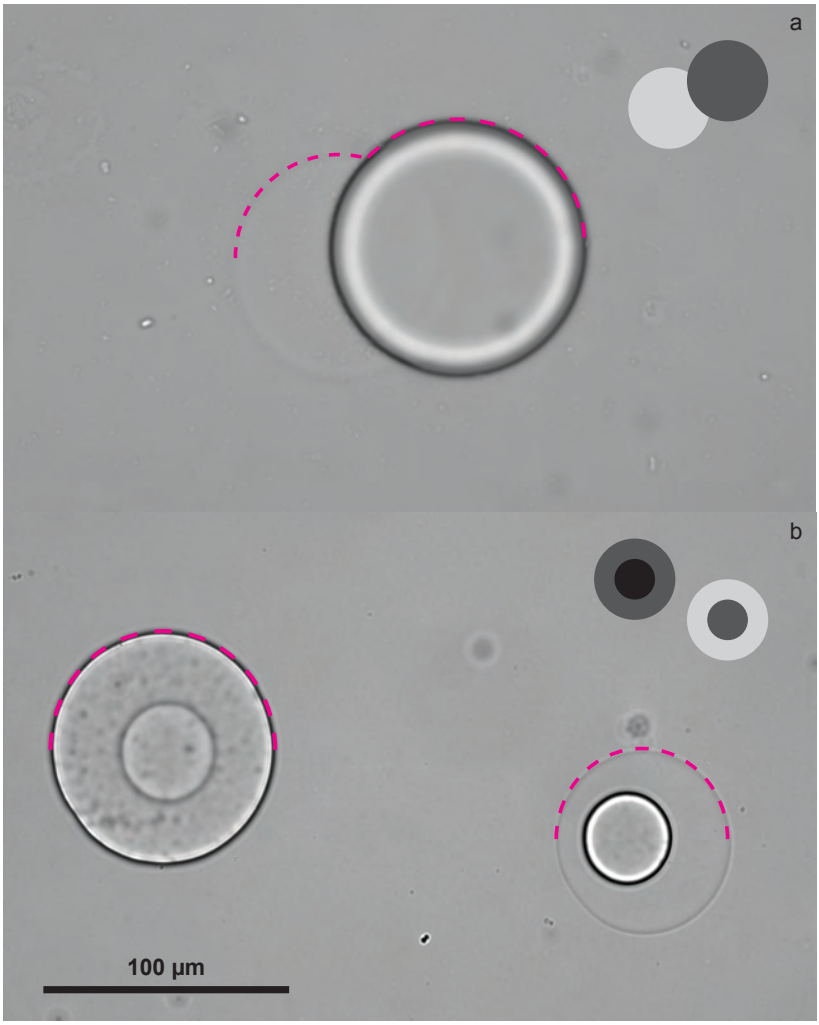

Fig. 4.10: Optical microscopy pictures of two different types of combinations of hard and soft post, with (a) a snowman post, where a soft post is attached to the side of a hard post and (b) omelette posts, where a hard and a soft post are synthesized around two smaller hard posts.

The omelette posts (figure 4.10b), solved this problem. The small hard posts ensured stability, as well as providing with a visual aid for aligning posts such that there could always be two posts visible, allowing for the hard and the soft post to be investigated at the same time. Therefore, these posts were used in all depletion experiments discussed in chapter 5.

5. RESULTS AND DISCUSSION PART 2: DEPLETION EXPERIMENTS

First steps were made towards putting all of the parts of the system together, by performing several experiments with posts inside channels. The results of these experiments are shown in figure 5.1. The horizontal dotted lines indicate the value that was calculated using the model as described in chapter 2. The results shown were averaged over six experiments, resulting in 500 to 2000 events per bar shown.

The diffusion value gives the time the particles need to diffuse through the medium without any interactions. This corresponds well with the theory from chapter 2. However, for the interactions with the posts, the measured values are unexpected. The escape time for the soft posts is much lower than the expected value, whereas the escape time for the hard post is much higher than the expected value. Furthermore, the standard deviation is very large.

When inspecting the time lapse, it was visible that there were particles getting stuck to the hard post, but not to the soft posts. The amount of stuck particles on the hard post and the soft post were counted for a representative experiment. The results are shown in figure 5.2. The amount of particles permanently stuck to the post is much higher on the hard post than on the soft post. A stuck particle would lead to an escape time on the order of magnitude of the length of the experiment (1 h), as the particle never escapes, which could explain the very long escape time as well as the large standard deviation.

Therefore, the data was analyzed again, but now a filter was applied, which filtered out all particles that were stuck irreversibly by dismissing all tracks that had an end value with a difference of less than one pixel from the begin value. The results of applying this filter are shown in figure 5.3. The value for the escape time from the hard post has shrunk considerably.

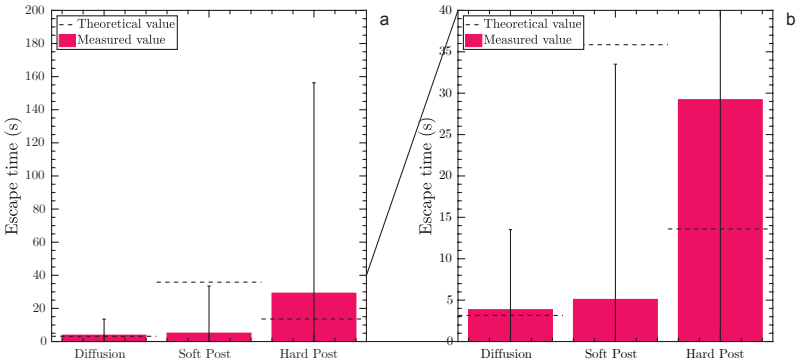

Fig. 5.1: Graph showing the measured escape time for soft and hard posts, as well as diffusion time. All where measured at $\phi = 0.05$. The results were averaged over five experiments. Figure (a) shows the complete results, figure (b) shows a cutout. The dashed line indicates the value that was expected from theory.

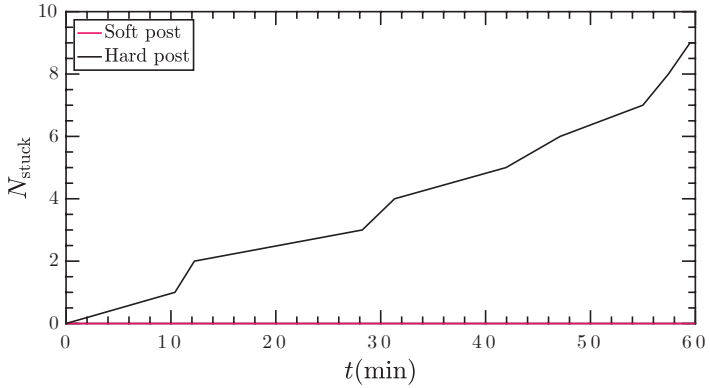

Fig. 5.2: The amount of particles stuck to a hard post (black) and a soft post (pink) in a representative experiment, measured over time.

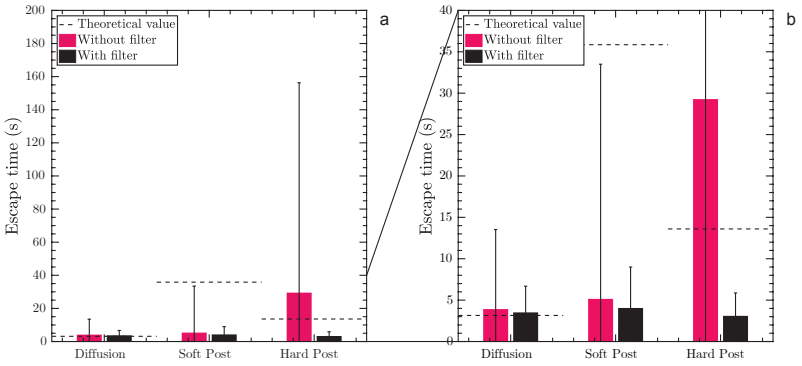

Fig. 5.3: Graph showing a comparison between the escape times where the analysis done without filtering out the particles that were irreversibly stuck (pink) and the analysis done with filtering out the particles that were irreversibly stuck (black). Figure (a) shows the complete results, figure (b) shows a cutout. The same data as in figure 5.1 was used.

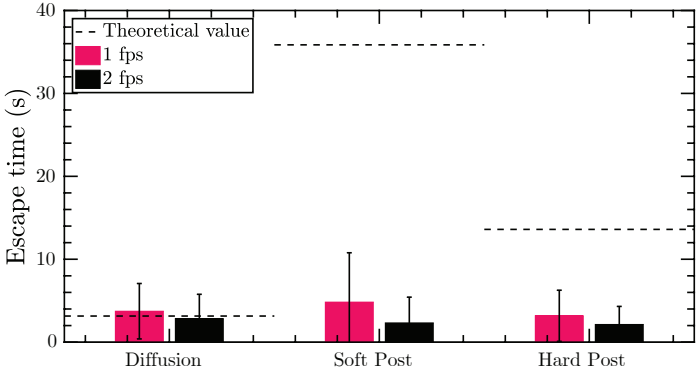

Fig. 5.4: Graph showing a comparison between the measured escape time where the analysis was done for all frames (resulting in 2 fps, black) or only for every other frame (resulting in 1 fps, pink). For this graph, three of the experiments that were used for figure 5.1 were taken into account.

When the stuck particles are filtered out, there is in fact no distinguishable difference between the measured escape time from the hard post, the soft post and the diffusion. Furthermore, the standard deviation is still quite large. It was proposed that the standard deviation might shrink with the frame rate used. In figure 5.4, the results for three experiments are shown, which were recorded at a frame rate of 2 frames per second. The analysis was done both for the 2 frames per second and 1 frame per second, by skipping every second frame. The results of this comparison are shown in figure 5.4. The value of the escape time does not change very much, nor does the error bar shrink considerably. The changes that are observed, can be accounted for by the fact that all tracks that were only a single frame in length, are counted as one second in 1 fps and as 0.5 seconds in 2 fps.

The effect of particles getting stuck to the hard post, but not the soft post, was investigated further. The hard post and the soft post are made from the same material, both consist of poly(ethylene)glycol diacrylate (PEGDA). The only big difference is the concentration of these materials. It was proposed that the hard post might have a lower crosslinking density than the soft post, leading to unspecified interactions from the dangling chains with the polystyrene particles. This in turn could lead to a second, deeper, energy minimum, leading to some of the particles getting irreversibly bound to the post.

Some experiments were done with hard posts, which were exposed for a different time. The amount of stuck particles were counted for $t = 0$ and $t = 60$ minutes. The results are shown in figure 5.5a. At least for these exposures, the exposure time does not have an influence on the amount of particles stuck. However, the effect does get stronger with depletant present, which suggests that there is a short range interaction going on. This does not refute our hypothesis that the second energy minimum could be caused by dangling chains.

It was proposed that the dangling chains would interact less with the particles if there were no more double bonds. To oxidize all the double bonds present, the posts were treated for 5 min with a 500 µmol L^{-1} solution of $KMnO_4$. The experiment was then repeated for two exposures. The results are shown in figure 5.5b. Treatment with $KMnO_4$ does not seem to have an effect. This could be because the $KMnO_4$ does not have the desired effect, or that oxidizing the double bonds is not the solution.

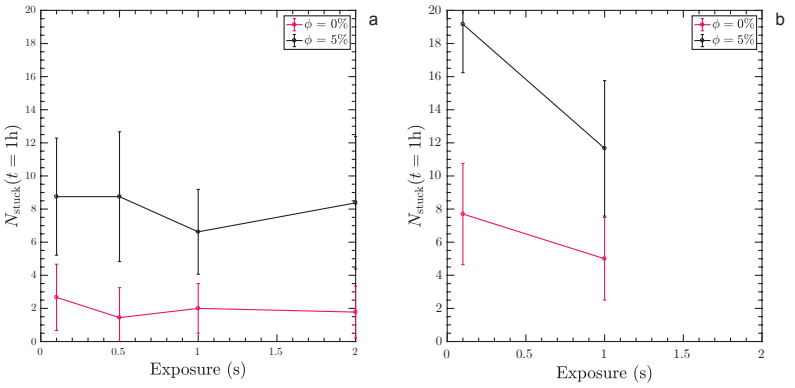

Fig. 5.5: Number of particles stuck to a hard post as a function of exposure time, comparing for $\phi = 0\%$ and $\phi = 5\%$, where in figure (a) the posts were not treated with $KMnO_4$ and in (b) the posts were treated with a $0.5\,\text{mmol}\,\text{L}^{-1}$ aqueous $KMNO_4$ solution for 5 minutes before adding particles.

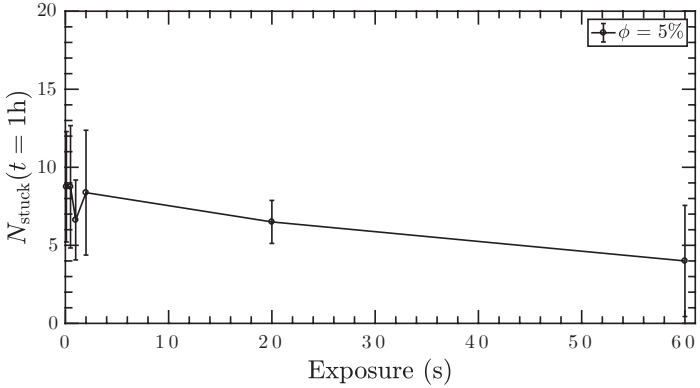

Fig. 5.6: Number of particles stuck after 1 hour as a function of exposure time

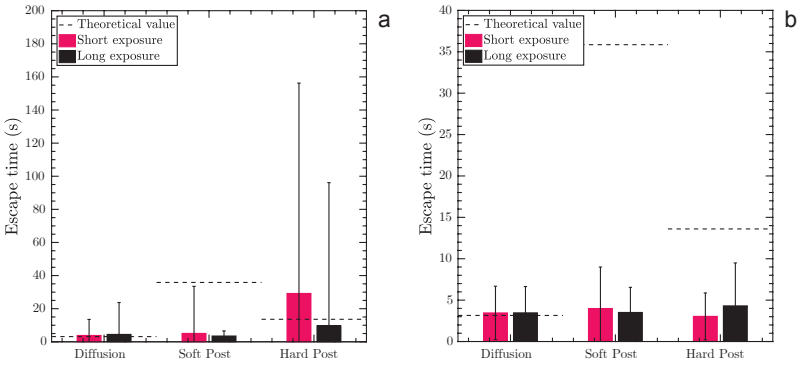

Fig. 5.7: The escape time for the soft and hard post, comparing posts made with a short exposure (soft: 2 seconds, hard: 0.5 seconds, pink) and a long exposure (both posts 60 seconds, black) where in (a) all particle tracks are taken into account and in (b) particles that got stuck permanently are filtered out.

It was proposed that the exposure times used were too short to achieve complete cross-linking, and the experiment was repeated with a very long exposure. These results are shown in figure 5.6. The longer exposure does seem to reduce the sticking effect, although it does not completely eliminate it. It could be due to the post still not being completely cross-linked at the edges, or that there are more unspecified interactions taking place.

The original depletion experiment was repeated, but now an exposure time of 60 seconds was used for both the soft and the hard posts. The soft post was illuminated for 2 seconds 30 times, with a waiting time of 0.5 seconds, the hard post was illuminated for 0.1 seconds 600 times, with a waiting time of 0.25 seconds. The results of this experiment are compared to the previous experiments in figure 5.7.

There is much less of a difference between the soft post and the hard post and between the values obtained with and without filtering out permanently stuck particles. Although more research needs to be done on what exactly causes the particles to get stuck, exposing longer might just be the right path.

The issue that remains, however, is that the escape time measured shows no real difference with the diffusion time. As written in section 3.5.3, the time for which $d < e$ is measured in MATLAB. We have assumed here that we can see the particle getting close, falling into the energy minimum and getting out again, resulting in tracks like 5.8a. Kraamer's escape time however, assumes that the particle is already in the energy minimum. Therefore, Kraamer does not take into account the diffusion time needed to get into the minimum. This is illustrated in figure 5.8b. This should lead to the measured escape time being slightly longer than what Kraamer predicts.

Since Kraamer only takes into account particles that have already fallen into the energy minimum, it does not take into account particles that just diffuse in region *ce*, with tracks like 5.8c. However, in the analysis these particles are being taken into account, resulting in shorter escape times than what Kraamer predicts. As long as the particles have to diffuse to the post, this can not be changed experimentally.

Furthermore, since the system used is not truly 2D, but rather a 3D system, particles do not only diffuse in the plane of focus, but also up and down. This results in particles moving into focus or out of focus while in the zone where we measure the escape time, leading to tracks like 5.8d. These tracks result in a measured escape time much shorter than the predicted value. It is expected that the effect of this practical issue is far greater than the effects mentioned before.

The time lapse was analyzed by hand. This proved that by eye, it might just be even harder to distinguish between particles interacting and diffusing. In the time lapse of an hour, less than 5 events of particles getting stuck reversibly were seen without a doubt, meaning that statistics are a real problem that needs to be addressed, should this research be continued.

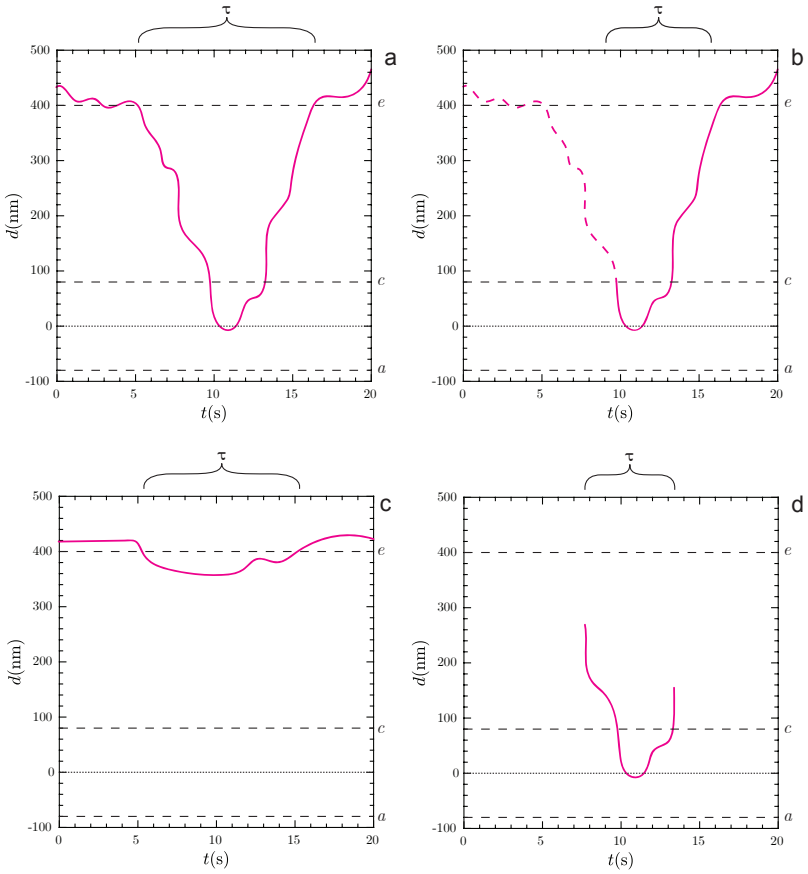

Fig. 5.8: Illustration of different types of tracks with (a) an ideal track as analyzed (b) the escape time that is predicted using Kraamer's method (c) a track that doesn't get into the energy well and (d) a track that is too short. The dotted line indicates where $d = 0$, the dashed lines show point e (particle completely escaped) and points a and c (the start and end of the energy well).

6. CONCLUSION AND OUTLOOK

Allostery is a type of adhesion process, where the substrate can be in multiple states, each with a different binding affinity for the adsorbent. Allosteric processes are one of the fundamental requirements for cell life, as almost all interactions involving proteins are allosteric. The term allostery was first coined in 1961 by Monod, who went on to deem allostery the "second secret to life", second only to the genetic code.

In this thesis, first steps were made towards building a model of allosteric processes on a colloidal scale. We used PEGDA posts with a tunable elasticity as our substrate and rigid polystyrene particles as our adsorbent. Depletion interaction modeled the binding of the particles to the substrate, the wall deforming modeled the conformation change.

Our theoretical model shows that indeed, the binding affinity depends strongly on the elasticity of the post. In fact, it showed that the system is extremely sensitive to very small changes in almost all important parameters. In experiments, these parameters should therefore be very well controlled.

By using larger depletant concentrations, the relative error in depletant concentration could be lessened. However, the real problem with the depletant is that its size is quite unsure. The weight range of the depletant used is large and therefore the range in radius of gyration is large. It might help to use a smaller depletant or one with a narrower size distribution. Another option might be to not use a polymer as a depletant at all, but synthesize or buy small spherical particles of the same order of magnitude. The size of this depletant could then be measured using TEM, to obtain an accurate size ratio of the particles and and the depletant.

Experiments showed that the elasticity could be tuned over 4 orders of magnitude. However, this is only the bulk value. The interface

between PEGDA and water could be studied more extensively by scaling up the system. Scaling up could be done by using bulk PEGDA to form an interface instead of the posts, thus eliminating all the issues arising with making posts. It would then be possible to just study the interface and the unspecified interactions that come with it. When using bulk PEGDA, it also becomes possible to study the cross-linking process over time using rheology.

Experiments showed a possible secondary energy minimum, which caused particles to get irreversibly stuck. We propose that this secondary minimum is due to an incomplete cross-linking density of the posts. Full cross-linking density could be achieved by illuminating the entire channel with UV light after it has been flushed with water or exposing for a longer time. Furthermore, it could be possible to use only PEGDA 6000 in experiments, eliminating any differences that might arise due to the different materials used. We could also use a lower concentration of PEGDA for the hard post, since rheology has shown that the post is already quite rigid at 8 %, hard posts could be achieved at concentrations as low as 10 % to 30 %, making it easier to achieve full cross-linking.

When analyzing the experiments, it became apparent that using the current method, the statistics are quite poor. In order to obtain a more reliable value for the escape time, and thereby the binding affinity, the statistics do need to be improved.

One of the routes could be to convert the 3D-system to a system that is closer to 2D. It might be possible to use much thinner channels which can be entirely in the depth of focus of the microscope. Using less thick channels might also help with the post making process, making posts less conical. However, the thinner the channel used, the harder it is to prepare the microfluidic device. Furthermore, particles interacting with the bottom or top of the channel would then become much more of an issue. Another way to get closer to a 2D system is by mismatching the density of the particles with the fluid, or making the particles much bigger, thus making them travel to the bottom of the glass faster. A polymer brush coating on the glass might be used to make sure that the particles do behave Brownian when they get to the bottom of the glass.

A different solution might be to increase the concentration of the particles, thus leading to more events and more statistics. However,

when the concentration gets too high, this could confuse the tracking software as single particles might be harder to distinguish.

Finally, it could be an option to try optical tweezers to force an event. Every single event would then have to be done by hand, but then we could assume that each measurement represented a particle getting into the shallow energy minimum, resulting in escape time values that should match the theoretical value as calculated by Kraamer's method more accurately.

In order to get closer to a true colloidal analogy for allosteric interactions, the system could be scaled down. Scaling down could be done by synthesizing smaller PEGDA posts, of the same order of magnitude as the polystyrene spheres. This system could then be studied to see if any collective behavior can be observed. For example, if the coverage over time looks more like a Langmuir curve or an MWC curve for different elasticities. Even more drastically, small spherical PEGDA particles with a tunable elasticity could be synthesized. This, however, would take an entirely new method of synthesis.

7. ACKNOWLEDGEMENTS

First and foremost, I would like to thank my team of supervisors. Willem, who came up with the idea for this research and was never too busy to nudge me in the right direction when I was stuck. Andrei, for inviting me to the candy club, which provided with a lot of useful discussions. Ivan, who never wanted to be called my supervisor, who babysat me when none of my other supervisors were around and proceeded to fix all of my silly little problems. I do not think we had a single discussion in which I did not learn something. Jasper, for guiding from afar, helping to make theory and statistics make sense. Finally, of course, Burak, who accidentally became my prime supervisor. Without your endless optimism and belief in my abilities, this master thesis would not have existed.

I would like the candy club, for all the useful discussions (and delicious candy). Thank you Chris for showing me how to use the optical microscopes, Anna, for helping me with the rheology measurements and Stijn, for helping me with DLS measurements. Bas is thanked for the help with the synthesizing and dyeing process of the polystyrene particles.

A big thanks also goes to my fellow master students for providing a nice support group and showing me that whatever obstacle I faced, I was not alone. Thank you FCC, for providing with a stimulating and friendly environment.

Thank you dad, mum and Chris, for always providing with a place to come home to and a listening ear, for both my triumphs and my frustrations. Last, but definitely not least, I would like to thank Dennis. You make every day just a little bit better, just by being you.

BIBLIOGRAPHY

[1] A. Kellar, "Mechanisms of Adhesion in Geckos," *Integr. Comp. Bio.*, vol. 1090, no. 42, pp. 1081–1090, 2002.

[2] J. Fröhlich-nowoisky, C. J. Kampf, B. Weber, J. A. Huffman, C. Pöhlker, M. O. Andreae, N. Lang-yona, S. M. Burrows, S. S. Gunthe, W. Elbert, H. Su, P. Hoor, E. Thines, T. Hoffmann, V. R. Després, and U. Pöschl, "Bioaerosols in the Earth system: Climate, health, and ecosystem interactions," *Atmospheric Research*, vol. 182, pp. 346–376, 2016.

[3] F. Donato, G. Garzaro, E. Pira, and P. Boffetta, "Mortality and cancer morbidity among cement production workers: a meta analysis," *International Archives of Occupational and Environmental Health*, vol. 89, no. 8, pp. 1155–1168, 2016.

[4] S. Marzen, H. G. Garcia, and R. Phillips, "Statistical Mechanics of Monod Wyman Changeux (MWC) Models," *Journal of Molecular Biology*, vol. 425, no. 9, pp. 1433–1460, 2013.

[5] C.-j. Tsai and R. Nussinov, "A Unified View of "How Allostery Works"," *PLOS Computational Biology*, vol. 10, no. 2, 2014.

[6] J. Liu and R. Nussinov, "Allostery : An Overview of Its History , Concepts , Methods , and Applications," *PLOS Computational Biology*, pp. 3–7, 2016.

[7] J. M. Berg, T. JL, and S. L., "Section 10.2, Hemoglobin Transports Oxygen Efficiently by Binding Oxygen Cooperatively," in *Biochemistry*, 5th ed., 2002.

[8] K. C. H. Bohr and A. Krogh, "Ueber einen in biologischer beziehung wichtigen Einfluss, den die kohlen- s{ä}urespannung

des blutes auf dessen sauerstoffbindung {ü}bt. Skandinavisches," *Skandinavisches Archiv Für Physiologie*, vol. 16, pp. 402–412, 1904.

[9] J. J. F. Monod, "General conclusions: telenomic mechanisms in cellular metabolism, growth, and differentiation.," *Quant Biol*, vol. 26, pp. 289–401, 1961.

[10] J. Monod, J. Wyman, and J. P. Changeux, "On the Nature of Allosteric Transitions: A Plausible Model.," *J Mol Biol*, vol. 12:, pp. 88–118, 1965.

[11] J. Monod, *Chance and Necessity: Essay on the Natural Philosophy of Modern Biology*. Penguin Books Ltd., 1977.

[12] H. N. W. Lekkerkerker and R. Tuinier, *Colloids and the Depletion Interaction*. Springer Berlin Heidelberg, 2011.

[13] W. K. Kegel, "Toy Models in physical chemistry and molecular biology," 2016.

[14] J.-P. Changeux, "Allostery and the Monod-Wyman-Changeux model after 50 years.," *Annual review of biophysics*, vol. 41, pp. 103–133, 2012.

[15] H. Z. An, H. B. Eral, L. Chen, B. Chen, and P. S. Doyle, "Soft Matter Synthesis of colloidal microgels using oxygen- controlled flow lithography ," *Soft Matter*, vol. 10, pp. 7595–7605, 2014.

[16] L. Yang, L. Zhu, Z. Li, and B. Lu, "Fabrication of PDMS microfluidic chips used in rapid diagnosis by micro jetting," *Multimedia Tools and Applications*, 2016.

[17] W. E. Uspal, H. B. Eral, and P. S. Doyle, "Flows using particle shape," *Nature Communications*, vol. 4, pp. 1–9, 2013.

[18] M. Mravlak and D. D. P. Ziherl, "Depletion force," *Department of Physics*, vol. PhD, 2008.

[19] V. L. Popov, "Contact Mechanics and Friction," 2010.

[20] K. K. Chawla, *Mechanical Behavior of Materials*. Prentice Hall, 1999.

[21] P. M. D. Molina, S. Lad, and M. E. Helgeson, "Heterogeneity and its influence on the Properties of Difunctional Poly(ethylene glycol) Hydrogels: Structure and Mechanics," *Macromolecules*, 2015.

[22] D. J. Kraft, R. Ni, F. Smallenburg, M. Hermes, K. Yoon, D. A. Weitz, and A. V. Blaaderen, "Surface roughness directed self-assembly of patchy particles into colloidal micelles," *PNAS*, 2012.

[23] D. J. Kraft, W. S. Vlug, C. M. Van Kats, A. Van Blaaderen, A. Imhof, and W. K. Kegel, "Self-assembly of colloids with liquid protrusions," *Journal of the American Chemical Society*, vol. 131, no. 3, pp. 1182–1186, 2009.

[24] R. Bhat and S. N. Timasheff, "Steric exclusion is the principal source of the preferential hydration of proteins in the presence of polyethylene glycols.," *Protein science: a publication of the Protein Society*, vol. 1, no. 9, pp. 1133–43, 1992.

Appendices

Appendix A

LIST OF ABBREVIATIONS AND SYMBOLS

Table A.1 provides with a list of abbreviations used in this thesis, table A.2 provides with a list of symbols used. It does not provide with the abbreviations of chemicals used, which can be found in table 3.1.

Tab. A.1: List of abbreviations

Abbreviation	Meaning
BF	Bright Field mode
CPS	Crosslinked Polystyrene particles
CPSR	Crosslinked Polystyrene particles, with Rhodamine
DLS	Dynamic light scattering
LPS	Linear Polystyrene particles
RITC	Fluorescence mode
TEM	Transmission Electron Microscopy
UV	Ultra-violet

Tab. A.2: List of symbols

Symbol	Units	Description
$\beta = (k_\mathrm{B}T)^{-1}$	J^{-1}	Inverse thermal energy
ϵ	$k_\mathrm{B}T$	Energy
ϵ_T	$k_\mathrm{B}T$	Binding energy in the tense state
ϵ_R	$k_\mathrm{B}T$	Binding energy in the relaxed state
ζ	m	Characteristic length
η	Pa s	Viscosity
Θ	–	Fraction of occupied binding sites
λ	–	Fugacity
Ξ	–	Grand canonical partition function
Π	$\mathrm{J\,m^{-3}}$	Osmotic pressure
τ	s	Escape time
ϕ	–	Volume fraction
ϕ_0	–	Volume fraction before mixing
$\phi_{0,\mathrm{p}}$	–	Percolation threshold
d	m	Distance between wall and face of particle
D	$\mathrm{m^2\,s^{-1}}$	Diffusion coefficient
E	$\mathrm{J\,m^{-3}}$	Elasticity
E	$k_\mathrm{B}T$	Total Energy
G_0	$\mathrm{J\,m^{-3}}$	Shear elastic modulus
G'	$\mathrm{J\,m^{-3}}$	Shear storage modulus
G''	$\mathrm{J\,m^{-3}}$	Shear loss modulus
h_E	m	Height of spherical cap
h_O	m	Height of spherical cap
k_B	$\mathrm{J\,K^{-1}}$	Boltzmann constant
n	–	Number of particles
n_b	$\mathrm{m^{-3}}$	Number density
r	m	Radius of particle
R_g	nm	Radius of gyration
T	K	Absolute temperature
U	$k_\mathrm{B}T$	Elastic energy
V_O	$\mathrm{m^3}$	Overlap volume
W	$k_\mathrm{B}T$	Depletion interaction energy

Appendix B

USING MATLAB TO DETERMINE THE ESCAPE TIME THEORETICALLY

MATLAB codes where used to calculate the escape time using the theoretical model developed in chapter 2. In section B.1, the code is shown that was used, where the depletion energy (B.2) and deformation energy (B.3) are calculated first, after which they are added together and used to calculate the escape time (B.4).

B.1 Main code

```
clear

%% Standard input variables

Na = 6.0221409*10^23;        %avogadros number in /mol
k = 1.38064852*10^-23;       %boltzmanns constant in J/K
T = 293;                     %temperature in K

r = 0.9*(10^-6);             %radius of particle in meters
R = 50*(10^-6);              %radius of post in meters
Rg = 20*(10^-9);             %radius of gyration in meters
Mr = 550000;                 %molar weight of depletant in g/mol
eta = 2.00*10^-3;            %viscosity of medium in Pa*s
phi = 0.05;                  %concentration
D = (k*T)/(6*pi*eta*r);      %calculating diffusion constant

E_standard = 1000;           %elasticity in Pa
E_points = [0.5*10^3:0.5*10^3:4.5*10^3 10*10^3:10*10^3:50*10^3];
%Points for calculating E in the loop (the more, the better,
%but watch computer time!)
```

```
ii=0; %starting value counter for outer loop
%(the points of elasticity)
jj=0; %starting value counter for inner loop
%(the points of the changed variable)

%% Section: the stuff you want to vary

var_label = 'r';  %the name of the variable you want to change
var_unit = '$\mu$m'; %the unit of the variable you want to change
step_v = 0.1*10^-6;  %define the stepsize with which you want to
%change the variable
num_v = [0.1*10^-6:step_v:1*10^-6]; %define the range with which
%you want to change the variable
order_v = 10^6; %factor to get from SI unit to variable unit
%(for example: nm = 10^9)

%% Calculating and plotting

for r = num_v
variable = r;

%% Defining some more stuff for the calculations

[cmap1,cmap2,cmap3,cmap4] = Colours(num_v);

stepsize = 1*10^-10;  %stepsize (keep tiny for accuracy!)

d = 0:stepsize:(R+2*r+2*Rg);            %absolute center to center
%distance in meters for the sphere and the wall
d_sph = (R+r):stepsize:(R+2*r+2*Rg);    %absolute center to center
%distance in meters for the spherical particles

drel = (d-R-r)/(2*r);               %converting center to center
%to wall to wall distance and making it relative to particle size
drel_sph = (d_sph-R-r)/(2*r);       %converting center to center
%to wall to wall distance and making it relative to particle size
%for the spherical particles

h_W = R+r+2*Rg-d;                   %converting distance to height
%for the formula for depletion
h_U = R+r-d;                        %converting distance to height
%for the formula for elastic energy
c = phi*(3/(4*pi*Rg^3))*(Mr/Na);    %converting phi to absolute
%concentration of depletant in g/m3 for formulas

%% The actual calculating and plotting
```

```
jj=jj+1;                                %counter for outer loop
ii=0;                                   %counter for inner loop

for E = E_points

ii = ii+1;
%counter for inner loop

[W, W_sph] = Depletionenergy(h_W,r,Rg,R,stepsize,c,Na,Mr,k,T);
%calculates the depletion energy in Joules
[U] = Deformationenergy(h_U,r,Rg,R,stepsize,k,T,E);
%calculates the depletion energy in Joules

Energy = U - W;
%calculates the total energy for sphere and wall
Energy_sph = -W_sph;
%calculates the total energy for spherical particles

minimum_elasticity(ii) = min(Energy);
%finds the minimum of the energy as a function of elasticity
minimum_elasticity_sph(ii) = min(Energy_sph);
%finds the minimum of the energy as a function of elasticity
%for the spherical particles

    if E == E_standard
%this part actually calculates for the variable you changed

       tau(jj) = Escapetime(Energy,d,R,r,k,T,eta,stepsize);
%calculates the escape time as function of the changed variable
       minimum_variable(jj)= min(Energy);
%finds the minimum of the energy as a function
%of the changed variable
       minimum_variable_sph(jj)=min(Energy_sph);
%finds the minimum of the energy as a function
%of the changed variable for the spherical particles

       legendInfo{jj} = sprintf('%s %s %.%s',...
       var_label,'=',variable*order_v,var_unit);
%gives the legendinfo for the changed variable

Figure3totalenergies(drel,drel_sph,Energy,Energy_sph,...
W,U,cmap1,cmap2,cmap3,cmap4,jj,legendInfo,k,T)
%figure 3: plots the total energy as a function of the distance
%for the changed variable

    end
```

```
end

Figure1energyminimaversuselasticity(E_points,minimum_elasticity,...
minimum_elasticity_sph,cmap1,jj,legendInfo,k,T)
%figure 1: plots the energy minimum as a function of the
%elasticity for the changed variables

end

% Figure2energyminimaversusvariable(num_v,order_v,cmap1,jj,...
minimum_variable,var_label,var_unit,k,T);
%plots figure 2: plots the energy minima versus
%the changed variable
Figure4escapetimeversusvariable(num_v,tau,cmap1,jj,...
var_label,var_unit,order_v);
%plots figure 4: plots the escape time versus
%the changed variable

Figure5escapetimeversusenergyminimum(minimum_variable,tau,...
cmap1,jj,k,T)
%plots figure 5: plots the escape time versus energy minima
%for changed variable

%%little piece of code to put in a dashed line at 0 in figure

figure(3)

y = get(gca,'ylim');
x = 0;
plot([x x],y,'k--','Linewidth',2);


%
```

B.2 Depletion energy

```
function [W,W_sph] = ...
Depletionenergy(h_W,r,Rg,R,stepsize,c,Na,Mr,k,T)

% sphere-wall

V1 = h_W.*0;
%overlap volume branch 1 in cubic meters
V2 = (1/3)*pi.*h_W.^2.*(3*(r+Rg)-h_W);
%overlap volume branch 2 in cubic meters
```

```
V3 = h_W.*0+4*pi*Rg*(r.^2+Rg*r+(1/3)*Rg.^2);
%overlap volume branch 3 in cubic meters

Vtotal = [V3(1:((R-r)/stepsize)) ...
            V2((R-r)/stepsize:(R+r+2*Rg)/stepsize) ...
            V1((R+r+2*Rg)/stepsize:(R+2*r+2*Rg)/stepsize)];

W = c*(Na/Mr)*Vtotal*k*T;
%calculates the depletion energy in Joules

%sphere-sphere

V1_sph = 0.5*V1;
%overlap volume branch 1 in cubic meters
V2_sph = 0.5*V2;
%overlap volume branch 2 in cubic meters

        Vtotal_sph = ...
            [V2_sph((R+r)/stepsize:(R+r+2*Rg)/stepsize) ...
            V1_sph((R+r+2*Rg)/stepsize:(R+2*r+2*Rg)/stepsize)];

W_sph = c*(Na/Mr)*Vtotal_sph*k*T;
%calculates the depletion energy in Joules


%
```

B.3 Deformation energy

```
function [U] = Deformationenergy(h_U,r,Rg,R,stepsize,k,T,E)

U1 = h_U.*0;
%deformation energy branch 1 in Joules
U2 = 8/15*E*r^(1/2)*h_U.^(5/2);
%deformation energy branch 2 in Joules
U3 = ((32*2^(1/2))/15)*E*r^3*h_U.^0;
%deformation energy branch 3 in Joules

U = [U3(1:(R-r)/stepsize) ...
            U2((R-r)/stepsize:(R+r)/stepsize) ...
            U1((R+r)/stepsize:(R+2*r+2*Rg)/stepsize)];
            %combines all branches to 1 vector

U_kT = U/(k*T);
%calculates the deformation energy in kT
```

B.4 Escape time

```
function [tau] = Escapetime(Energy,d,R,r,k,T,eta,stepsize)

ac = find(Energy <= 0);              % indices where E <= 0
b = find(Energy == min(Energy));     % index where E = minimal
e = find(d == R+r+401*10^-9);        % index where d = 400nm

E1 = Energy(ac); % values of u for the indices ac
E1exp = exp(-E1./(k*T)).*stepsize; % convert to exponential
Well = sum(E1exp); % 'integrate'

E2 = Energy(b:e); % values of u in the index range b to e
E2exp = exp(E2./(k*T)).*stepsize; %convert to exponential
Escape = sum(E2exp); %'integrate'

tau = (6*pi*eta*r)/(k*T)*Well*Escape %calculates the escape time
```

Appendix C

USING MATLAB TO DETERMINE THE ESCAPE TIME EXPERIMENTALLY

MATLAB codes were used to determine the escape time experimentally. The first code, in section C.1 puts the .tif files of the ND aquisiton in order and then tracks them. The complete tracking code was written by Pepijn Moerman and can be provided. The next code, section C.2, uses the tracking to determine escape times, where C.3 makes the tracks relative to the post postitions and C.4 is the code which is used to actually calculate the escape time.

C.1 Auto tracking

```
%-----This file automatically runs trackingcode.m
% for every tiff file.
%-----Can also split the track into parts,
%if so desired.

clear

tic

Escapetime = [];
lx = [];
pos = [];

framenumber = 0;
for jjj = 1:7
    dir = 'G:\Analysis\1051013\';
```

```
    fname = sprintf('%s1051013%i.tif',dir,jjj);
    fsave = sprintf('%soutput 1051013 1fps%i.txt',dir,jjj);
    run trackingcode.m

    clearvars -except jjj Escapetime filename lx pos ...
    framenumber maxdisp param fsave

end

tr=track(pos(1:end,:),maxdisp,param);

%type filename under which you want to save results
textfile=[tr];
fileID = fopen(fsave,'w');
%fprintf(fileID , '%6s %6s %6s %6s \n' , 'x' , ...
'y'  ,'time' , 'partID');
fprintf(fileID , '%6.4f %6.4f %6.4f %6.4f \n' , textfile');
fclose(fileID);

toc



%
```

C.2 Analysis

```
clear

tic

Escapetime = [];
lx = [];
pos = [];
qq = 0;
%the code below creates a result file with a header
Resultnames = {'Sample','fps','softbulk','softbulkstd',...
'hardbulk','hardbulkstd','soft','softstd','hard','hardstd'};
Results = [];
Distributions = [];

posfile = 'G:\Analysis\postpositions.txt';
%gets the post positions
postpositions = textread(posfile);
%reads the file post positions
```

```
for Expno = [93103 93104 93105 93107 95102 95104]
%this can be used to process multiple experiments at once

    for Fpsno = [1 2];
    %this defines what framerate (specified in .txt) is used
        try

fsave = sprintf('G:/Analysis/%i/%ifps%i.txt',Expno,Expno,Fpsno);
fresults = sprintf('G:/Analysis/totalresultswithoutfilter.txt');
input=textread(fsave);   %gets the tracking data
Softie = str2num(sprintf('%i%i',Expno,1));
Hardie = str2num(sprintf('%i%i',Expno,0));

% The code below finds the hard posts
postx = postpositions(postpositions(:,1)==Hardie,2);
posty = postpositions(postpositions(:,1)==Hardie,3);
ringstart = postpositions(postpositions(:,1)==Hardie,4);
ringend = ringstart + 12;
run Relativetopost.m %this makes tracking relative to post
hardTau = mean(Escapetime)/Fpsno;
hardTaustdev = std(Escapetime)/Fpsno;

qq = qq+1;
fdistr = sprintf('G:/Analysis/distribution_hardpost%i_%i.txt',...
Expno,Fpsno);
fileID = fopen(fdistr,'w');
fprintf(fileID , '%i ' , Escapetime');
fclose(fileID);

Escapetime = [];

ringstart = ringstart + 20;
ringend = ringstart + 12;
run Relativetopost.m
hardbulkTau = mean(Escapetime)/Fpsno;
hardbulkTaustdev = std(Escapetime)/Fpsno;

fdistr = sprintf('G:/Analysis/distribution_hardbulk%i_%i.txt',...
Expno,Fpsno);
fileID = fopen(fdistr,'w');
fprintf(fileID , '%i ' , Escapetime');
fclose(fileID);
Escapetime = [];

% soft posts now
postx = postpositions(postpositions(:,1)==Softie,2);
```

```
posty = postpositions(postpositions(:,1)==Softie,3);
ringstart = postpositions(postpositions(:,1)==Softie,4);
ringend = ringstart + 12;
run Relativetopost.m
softTau = mean(Escapetime)/Fpsno;
softTaustdev = std(Escapetime)/Fpsno;

fdistr = sprintf('G:/Analysis/distribution_softpost%i...
_%i.txt',Expno,Fpsno);
fileID = fopen(fdistr,'w');
fprintf(fileID , '%i ' , Escapetime');
fclose(fileID);
Escapetime = [];

ringstart = ringstart + 20;
ringend = ringstart + 12;
run Relativetopost.m
softbulkTau = mean(Escapetime)/Fpsno;
softbulkTaustdev = std(Escapetime)/Fpsno;

fdistr = sprintf('G:/Analysis/distribution_softbulk%i_...
%i.txt',Expno,Fpsno);
fileID = fopen(fdistr,'w');
fprintf(fileID , '%i ' , Escapetime');
fclose(fileID);

Results = [Results ; Expno, Fpsno, softbulkTau,...
softbulkTaustdev, hardbulkTau, hardbulkTaustdev,...
softTau, softTaustdev, hardTau, hardTaustdev];

        catch

            display('File not found. Continuing...');
            %in case the file is mistyped or does not exist

        end
    end
end

%save all values for Tau

fileID = fopen(fresults,'w');
fprintf(fileID , '%6.0f %6.0f %6.4f %6.4f %6.4f %6.4f ',...
'%6.4f %6.4f %6.4f %6.4f\n' , Results');
fclose(fileID);

toc
```

C.3 Relative to post

```
N_particles = max(input(:,4));
% Number of particle tracks

% N_particles = 5;
%can be used to only analyse some tracks instead of all of them

for j = 1:N_particles

    % for i = 3
    %can be used to analyse a specific track

track{j} = input(input(:,4)==j,:);
%splits the table into N tracks
x{j} = track{j}(:,1)-postx;
%x-coordinates of each track
lx = [lx size(cell2mat(x(j)),1)];

y{j} = track{j}(:,2)-posty;
%y-coordinates of each track
t{j} = track{j}(:,3);
%time points of each track
t_min{j} = min(t{j});
t_max{j} = max(t{j});
n{j} = track{j}(:,4);
% particle number, for completeness
trackrel{j} = cell2mat({x{j},y{j},t{j},n{j}});
% i = particle  number

dist{j} = cell2mat({sqrt(x{j}.^2+y{j}.^2),t{j}});
%calculates distance to center of mass
```

C.4 Escape time calculation

```
for ii = 1:N_particles

    if mean(abs(diff(dist{j}(:,1)))) >= 1  ...
    %this filters out the particles which are permanently stuck

        A = [];
        A(:,1) = dist{j}(:,1);
        A(:,2) = 0;

        for j = 1:length(A) %for the length of the track

            %the loop below gives a 1 for each number that is
            inside the ring

            if  A(j) <= ringend && A(j) >= ringstart
                A(j,2) = 1;
            end

        end

        C = A(:,2); %gets the second column of A
        D = diff([0 C' 0]); %calculates the length of
        %consecutive 1's (= time)

        Escapetime = [Escapetime find(D<0)-find(D>0)]; %puts all
        %the escape times in one matrix:

        %calculates the average escape time for the whole
        %ND aquisition

        Tau = mean(Escapetime);
        Taustdev = std(Escapetime); %calculates the standard
        %deviation

    end
end
```